DEVELOPMENTAL AND EVOLUTIONARY COMPARATIVE ANALYSIS OF A REGULATORY LANDSCAPE IN MAMMALS AND BIRDS

Aurélie Hintermann[1], Isabel Guerreiro[1,a], Christopher Chase Bolt[2], Lucille Lopez-Delisle[2], Sandra Gitto[1], Denis Duboule[1,2,3,#] and Leonardo Beccari[1,b]

Short title: Regulation evolution at the *HoxD* locus

Keywords: Chromatin topology, TAD, enhancers, evolution, gene regulation, development, teguments, placodes

[1]Department of Genetics and Evolution, University of Geneva, 30 quai Ernest-Ansermet, 1211, Geneva, Switzerland.

[2]School of Life Sciences, Federal School of Technology (EPFL), 1015 Lausanne, Switzerland.

[3]Collège de France, 75005 Paris, France.

[a]Present address: Oncode Institute, Hubrecht Institute-KNAW and University Medical Center Utrecht, Utrecht, The Netherlands.

[b]Present address: Institut Neuromyogène. CNRS UMR 5310, INSERM U1217, University of Lyon, Lyon, France.

[#]Corresponding author

Denis Duboule

Denis.Duboule@unige.ch

32

ABSTRACT

34

35   Modifications in gene regulation during development are considered to be a driving force in the
36 evolution of organisms. Part of these changes involve rapidly evolving *cis*-regulatory elements (CREs), which
37 interact with their target genes through higher-order 3D chromatin structures. However, how such 3D
38 architectures and variations in CREs contribute to transcriptional evolvability remains elusive. During
39 vertebrate evolution, *Hox* genes were redeployed in different organs in a class-specific manner, while
40 maintaining the same basic function in organizing the primary body axis. Since a large part of the relevant
41 enhancers are located in a conserved regulatory landscape, this gene cluster represents an interesting paradigm
42 to study the emergence of regulatory innovations. Here, we analysed *Hoxd* gene regulation in both murine
43 vibrissae and chicken feather primordia, two mammalian- and avian-specific skin appendages which express
44 different subsets of *Hoxd* genes, and compared their regulatory modalities with the regulations at work during
45 the elongation of the posterior trunk, a mechanism highly conserved in amniotes. We show that in the former
46 two structures, distinct subsets of *Hoxd* genes are contacted by different lineage-specific enhancers, likely as
47 a result of using an ancestral chromatin topology as an evolutionary playground, whereas the regulations
48 implemented in the mouse and chicken embryonic trunk partially rely on conserved CREs. Nevertheless, a
49 high proportion of these non-coding sequences active in the trunk appear to have functionally diverged
50 between the two species, suggesting that transcriptional robustness is maintained despite a considerable
51 divergence in CREs' sequence, an observation supported by a genome-wide comparative approach.

52

53

INTRODUCTION

55   Changes in the spatial and temporal regulation of genes critical for developmental processes have greatly contributed to the evolution of animal morphologies (see for example (Carroll, 2008; Rebeiz et al., 2015). The expression of such genes is generally modulated by combinations of *cis*-regulatory elements (CREs), short DNA sequences enriched for transcription factor binding sites, which tend to evolve more rapidly than the genes they control (Edwards et al., 2013; Long et al., 2016; Spitz and Furlong, 2012). CREs can be spread over large distances around the gene(s) they regulate, which gives to the spatial organization of chromatin a particular importance. Indeed, the existence of such 'regulatory landscapes' (Spitz et al., 2003) implies that enhancer-promoter interactions involve spatial proximity, which is generally thought to occur through large chromatin loops (Rao et al., 2014).

64   The extent of regulatory landscapes often correspond to Topologically Associating Domains (TADs) (Andrey et al., 2013; Harmston et al., 2017), which were defined as chromatin domains where the probabilities of interactions, as measured by chromosome conformation capture (Belton et al., 2012), are higher than when compared to the neighbouring regions (Dixon et al., 2012; Nora et al., 2012; Sexton et al., 2012). The distribution of TADs tends to be conserved in various vertebrate species, a phenomenon likely associated with regulatory constraints exerted by the complex and pleiotropic regulations found around many vertebrate developmental genes. Such domains, where many interactions might occur, were proposed to form particular chromatin niches, rich in various DNA-binding proteins and where the evolutionary emergence of novel regulatory sequences could be favoured due to the presence of both a pre-existing scaffold and appropriate co-factors (see (Darbellay and Duboule, 2016a). While genomic rearrangements altering the structure of TADs were reported to impact proper gene regulation during development, sometimes leading to genetic syndromes (e.g. (Bolt et al., 2021a; Bompadre and Andrey, 2019; Lupianez et al., 2015), in most cases, these rearrangements also affected enhancer-promoter spatial relationships, which makes a causal assessment difficult.

78   Genome-wide analyses carried out in different species, comparing DNA sequence conservation, TAD organization, or some epigenetic modifications, have started to reveal some of the molecular mechanisms underlying both the evolution of gene regulation and, by extension, the modification of species-specific traits. However, integrated functional approaches are required to better understand how changes in chromatin architecture and modifications in CREs may influence the evolvability and the robustness of gene transcription. To try to address such questions, we have used the *HoxD* locus as a paradigm of pleiotropic regulation of a multi-gene family, with a strong impact both on the control of important developmental steps, and on the emergence of evolutionary novelties. The *HoxD* cluster contains a series of genes in *cis*, which encode transcription factors that are expressed in different combinations across several embryonic structures. The cluster is flanked by two large TADs, each one matching a gene desert highly enriched in CREs (Darbellay and Duboule, 2016a). These two TADs are separated by a boundary region which is localized within the

3

89   cluster, close to its centromeric extremity (Andrey et al., 2013; Rodriguez-Carballo et al., 2017). The telomeric

90   TAD comprises a large number of enhancers controlling transcription of various *Hoxd* genes in most of the

91   tissues where HOX proteins operate (Andrey et al., 2013; Darbellay et al., 2019; Delpretti et al., 2013;

92   Guerreiro et al., 2016; Schep et al., 2016). In contrast, the centromeric TAD contains enhancers specific for

93   terminal structures such as digits or external genitals (Amândio et al., 2020; Montavon et al., 2011).

94   Amongst the many tissues where *Hoxd* genes exert a function are embryonic primordia of different

95   skin derivatives, including those of mammary glands, vibrissae and pelage hairs of mammals as well as those

96   of chicken feathers (Kanzler et al., 1997, 1994; Reid and Gaunt, 2002; Reynolds et al., 1995; Schep et al.,

97   2016)(Fig. 1). Despite the fact that these ectodermal structures share common developmental mechanisms and

98   gene regulatory networks such as the *Wnt*, EDA and BMP signaling pathways (Biggs and Mikkola, 2014;

99   Dhouailly et al., 2019; Di-Poï and Milinkovitch, 2016; Pantalacci et al., 2008; Wu et al., 2004), each type of

100   primordium expresses different subsets of contiguous *Hoxd* genes. Since the specific topological organization

101   of the *HoxD* locus can be observed in fishes (Acemel et al., 2016) (see Fig. S1A), it likely predates the

102   emergence of hairs and feathers during amniote evolution (Dhouailly, 2009; Wu et al., 2004). For this reason,

103   these organs represent valuable models to understand how CRE evolution within a pre-existing chromatin

104   architecture could lead to the implementation of new gene-specific expression patterns. In contrast, the general

105   organization of *Hoxd* gene expression along the main embryonic body axis is overall maintained across

106   vertebrate species, in spite of the low sequence conservation observed, raising the question as to how evolving

107   *Hox* clusters could maintain globally similar transcriptional outputs.

108   In this study, we addressed these issues by taking a comparative look at a well-defined regulatory

109   landscape, positioned telomeric to the *HoxD* gene cluster, in mammals and in birds. These two syntenic regions

110   contain CREs involved either in the same regulatory tasks, or controlling regulatory aspects specific to each

111   taxon. In the latter context, we characterized *Hoxd* gene regulation in the mouse-specific vibrissae primordia

112   (VPs) and in the chicken-specific feather primordia (FPs). We show that different subsets of contiguous *Hoxd*

113   genes are expressed in the mouse VP mesoderm and in the chicken FP ectoderm, indicating an independent

114   co-option of *Hoxd* paralogs in these structures. While the transcription of these genes in VPs and FPs relies on

115   lineage-specific CREs located within different segments of the regulatory landscape, these CREs exploit a

116   largely conserved chromatin 3D architecture.

117   Our comparative analysis of the regulation at work during trunk extension also revealed that *Hoxd1*

118   displays an expression pattern markedly different from that of its neighboring paralogs, both in mouse and

119   chick, and that this *Hoxd1*-specific expression is driven by an evolutionary conserved CRE located in a region

120   predominantly interacting with *Hoxd1* in both species. However, the cis-regulatory code at work in the latter

121   regulation differs between the two species, illustrating the possibility that inter-species conservation of both

122   gene transcriptional specificity and chromatin architectures are compatible with a high plasticity of the *cis*-

123   regulatory sequences involved. The extension of this observation genome-wide suggests that conserved CRE

124   sequences more frequently diverge in their regulatory activities than they conserve their functionality.

4

125

RESULTS

127

Different *Hoxd* gene expression in mammalian and avian skin appendages.

We initially analyzed the expression profiles of *Hoxd* genes in mouse VPs and chicken FPs (Fig. 1). Skin appendage development starts with the interaction of the skin ectoderm with its underlying mesoderm, resulting in the thickening of the epithelium into a placode and in the condensation of dermal cells into a papilla (Mikkola, 2007; Sawyer and Knapp, 2003; Widelitz and Chuong, 1999). VP development starts at early embryonic day 12 (E12), forming a stereotyped array of eight columns and five rows of VPs (Wrenn and Wessells, 1984)(Fig. 1A). The epithelial placode subsequently invaginates and engulfs the dermal papilla forming the follicle primordium (Fig. S1). Likewise, in birds, ectoderm-mesoderm interactions result in the evagination of feather buds around embryonic day 7 (stage HH30-32 (Hamburger and Hamilton, 1951; Michon et al., 2007) (Fig. S2).

Whole-mount *in situ* hybridization (WISH) revealed strong *Hoxd1* expression in the dermal papillae of the VPs (Fig. 1B; Fig. S1). Furthermore, a comparative analysis of VPs from single E12.5 embryos revealed that *Hoxd1* transcripts accumulate slightly after ectodermal placode formation, marked by the expression of *Shh* (Chiang et al., 1999) (Fig. S1). *Hoxd3* and *Hoxd4* are also expressed in VPs, yet at much lower levels than *Hoxd1* (Fig. 1B, Fig. S1). Faint levels of *Hoxd8* mRNAs were sporadically detected in the VPs, while *Hoxd9* and more 5'-located *Hoxd* mRNAs were never observed in these structures (Fig. 1B, Fig. S1). *In situ* hybridization on cryostat sections confirmed that *Hoxd1* transcripts accumulate in the dermal mesenchyme of VPs, but not in the ectoderm-derived portion of the follicle (Fig. S1). Therefore, *Hoxd1-Hoxd4* are transcriptionally active in the dermal papillae of developing VPs, with *Hoxd1* being the main paralog expressed in these structures.

WISH experiments in HH35 chicken embryos revealed expression of *HOXD3*, *HOXD4, HOXD8* and *HOXD9* in the FPs, while *HOXD1* and *HOXD11* mRNAs were not detected (Fig. 1C, D, Fig S2). Cryostat sections indicated that *HOXD* gene expression in chicken FPs is localized in the follicle ectoderm (Fig. S2), in contrast with murine VPs. Different *Hoxd* genes thus operate in dermal papillae of mouse VPs and in ectodermal placodes of chicken FPs, likely reflecting the implementation of different regulatory mechanisms in the two lineages.

154

***Hoxd* gene expression in the mouse and chicken embryonic body axis.**

Hox genes are expressed in the paraxial and lateral mesoderm of the main embryonic axis, as well as in the neural tube, and display a progressively more restricted expression domain depending on their position within the cluster (Gaunt et al., 1988). Comparative WISH analysis of mouse and chicken embryos revealed that *Hoxd1* expression patterns in the trunk were markedly similar between the two species, yet largely divergent from that of the 5'-located neighbor *Hoxd* paralogs (Fig. 1E-G). While *Hoxd4* was strongly and

5

161 uniformly transcribed in the mouse paraxial and lateral mesoderm as well as in the neural tube, *Hoxd1*

162 displayed a biphasic expression pattern. Transcripts accumulated in the embryonic tailbud, yet they rapidly

163 disappeared from the presomitic mesoderm and remained undetected in lateral mesoderm progenitors or in the

164 neural tube (Fig. 1F). Instead, *Hoxd1* was specifically re-activated during somite condensation, coupling the

165 transcription of this gene to the segmentation clock (Dale and Pourquié, 2000; Zákány et al., 2001). Similar to

166 the mouse pattern, the chicken *HOXD1* expression also differed from its neighbouring paralogs, even though

167 its transcripts remained detectable in the formed somites all along the main body axis (Fig. 1G). These

168 observations suggested that *Hoxd1* transcription in developing somites may depend on a specific set of CREs,

169 different from CREs controlling the neighboring paralogs, and that this locus-specific transcription was

170 evolutionarily conserved across amniotes.

171

172 **An evolutionary conserved topology at the *HoxD* locus.**

173 In order to see whether these differences and similarities in regulatory specificities could be associated

174 to variations in the global chromatin architecture at this locus, we performed Capture Hi-C (CHi-C)

175 experiments using dissected mouse and chicken posterior trunks (Fig. 2A, B). Even though the global size of

176 TADs at this locus is approximately two times smaller in the chicken genome, the *HOXD* region closely

177 resembled its mouse counterpart, with the T-DOM being further organized into two sub-TADs in both species

178 (Fig. 2, sub-TAD1 and sub-TAD2) (Rodríguez-Carballo et al., 2020; Yakushiji-Kaminatsui et al., 2018). Of

179 note, the presence and relative distribution of conserved non-coding elements (CNEs) were maintained within

180 this similar chromatin architecture (Fig. 2, Fig. S3).

181 We corroborated these observations by assessing the interactions established by the *Hoxd1*, *Hoxd4*

182 and *Hoxd9* promoters in mouse and chicken embryonic posterior trunk cells, using 4C-seq (Fig. S3). As an

183 indication for non-tissue-specific interactions, we used embryonic brain cells where *Hox* genes are not

184 transcribed. In both species, the three viewpoints established frequent contacts with the T-DOM while

185 interactions with the C-DOM were virtually absent. In addition, all viewpoints contacted T-DOM sub-TAD1

186 with a higher probability than T-DOM sub-TAD2, showing specific and non-overlapping regions where

187 interactions were enriched. *Hoxd1* contacted the first half of sub-TAD1 (Figs. 3A and S3, region D1), more

188 intensively than *Hoxd4* or *Hoxd9* (Fig. S3). In turn, *Hoxd4* contacts within the 3' half of sub-TAD1 (Figs. 3A

189 and S3, region D4), were increased up to the sub-TAD boundary (Fig. S3). Finally, *Hoxd9* interactions were

190 mostly limited to the sub-TAD boundary region (Figs. 3A and S3, region D9), where they were higher than

191 for *Hoxd1* and *Hoxd4*. This distribution of interacting regions within the 3' TAD were found in both brain and

192 posterior trunk cells, yet with an overall lower contact frequency in brain cells, reflecting the transcription-

193 independent default conformation of the region, in agreement with previous reports (Andrey et al., 2013;

194 Dekker and Heard, 2015; Noordermeer et al., 2011).

195 Chromatin architectures partly rely upon the presence of the zinc-finger DNA binding protein CTCF,

196 which together with the cohesin complex can induce the formation and stabilization of large loops. (Hansen et

6

197   al., 2017; Nanni et al., 2020; Pugacheva et al., 2020). The ChIP-seq analysis of the CTCF profiles revealed

198   that both at the mouse and chicken *HoxD* loci, the telomeric end of the D1 region maps close to an occupied

199   CTCF site (Fig. S3, blue arrowhead). Also, a cluster of CTCF binding sites delimits the boundary between the

200   mouse and the chicken sub-TAD1 and sub-TAD2 (Rodriguez-Carballo et al., 2017; Rodríguez-Carballo et al.,

201   2020; Yakushiji-Kaminatsui et al., 2018) thus correlating with the limit between the *Hoxd4* and *Hoxd9*

202   interacting D4 and D9 regions in both species (Fig. 2; Fig. S3, blue arrowheads in panel B).

203   Overall, these results show that *Hoxd1*, *Hoxd4* and *Hoxd9* preferentially interact with different

204   portions of the T-DOM and that these segments are somehow determined by the distribution of CTCF binding

205   sites in T-DOM subTAD-1. These distinct interactions patterns are constitutive and conserved between mouse

206   and chicken. From these results, we concluded that the evolutionarily conserved contact topology of *Hoxd*

207   genes with T-DOM may contribute to the implementation of their specific regulatory strategies in mouse and

208   chicken embryonic structures.

209

210   **Tissue-specific regulatory sequences are located in regions of preferential interactions**

211   To evaluate whether the promoter-specific partition of contacts with T-DOM is associated with the

212   presence of differential regulatory activities, we set up to identify the CREs controlling *Hoxd* gene expression

213   in the VPs, FPs and the embryonic trunk of both mouse and chicken embryos. We carried out ChIP-seq

214   analyses using an antibody against H3K27ac, a histone modification indicative of an active chromatin state

215   (Creyghton et al., 2010; Rada-Iglesias et al., 2011) and annotated tissue-specific regions with increased density

216   of H3K27ac enrichment referred to as MARs (Most Acetylated Regions, Fig. 3). MARs were identified as

217   genomic regions accounting for the highest H3K27ac enrichment after subtraction of the corresponding signal

218   in brain cells (see material and methods).

219   In the mouse VPs, the MAR mapped within the D1 region (Fig. 3A, top, red-filled rectangle), in

220   agreement with the stronger expression of *Hoxd1* compared to its neighbouring paralogs (Fig. 1B; Fig. S1).

221   Instead, in chicken dorsal skin samples where *HOXD1* is not active (Fig. 1D), the MAR largely overlapped

222   the D4 and the D9 interacting regions (Fig. 3A, bottom, red-filled rectangle). Therefore, VPs and FPs display

223   different distributions of H3K27ac enrichment across T-DOM, in agreement with the various sibsets of *Hoxd*

224   gene expressed in these tissues. In contrast, the MARs of both mouse and chicken posterior trunk samples

225   largely overlapped the D4 region (Fig. 3B, red-filled rectangles) as expected from their similar expression

226   patterns in the embryonic trunk of both species, with the expression domain of *Hoxd4* being more extended

227   than that of *Hoxd9* (Fig. 1F). In summary, the different enrichments of H3K27ac marks across T-DOM were

228   located within the genomic segments that preferentially interacted with the genes expressed in each tissue.

229

230   ***Hoxd1* regulation in mutant regulatory landscapes**

231   To evaluate the functional importance of the D1 interacting region, we assessed *Hoxd1* transcription

232   in different mouse lines carrying mutations affecting this regulatory domain. We first analyzed *Hoxd1*

233   expression in the VPs of mouse embryos carrying various deletions of T-DOM (Fig. 4A, red lines). In the

234   *HoxD$^{Del(attP-TpSB2)lac}$* allele, the D1 region is removed (hereafter referred to as *Del(attP-SB2)*. Since *Del(attP-*

235   *SB2)* homozygous embryos are not viable due to the deletion of the essential *Mtx2* gene (Andrey et al., 2013),

236   we crossed this line with the mouse line *HoxD$^{Del(1-13)d9lac}$* (Spitz et al., 2001), hereafter referred to as *Del(1-13)*.

237   In the latter line, the entire *HoxD* cluster is deleted, such as to be able to see the effect of the *HoxD$^{Del(attP-SB2)lac}$*

238   deletion upon *Hoxd* gene regulation in *cis*. *Hoxd1* expression in the VPs of trans-heterozygous *HoxD$^{Del(attP-}$*

239    $^{TpSB2)lac/Del(1-13)}$ mutant embryos was completely abolished, in contrast with *Del(1-13)* heterozygous control

240   littermates (Fig. 4B). Conversely, the *HoxD$^{Del(TpSB2-TpSB3)lac}$* allele (hereafter *Del(SB2-SB3)*(Andrey et al., 2013))

241   carries a large deletion that encompasses the whole T-DOM except the D1 region. We detected robust *Hoxd1*

242   expression in the VPs of E12.5 *HoxD$^{Del(TpSB2-TpSB3)lac/Del(1-13)}$* trans-heterozygous mutant embryos (Fig. 4B).

243   We complemented these results by producing mouse transgenic embryos carrying bacterial artificial

244   chromosomes (BACs) spanning the *HoxD* cluster and/or parts of sub-TAD1 (in blue in Fig. 4A). In agreement

245   with the analysis of the T-DOM deletions, the BACs covering either the *HoxD* cluster (BAC^{HoxD} (Schep et al.,

246   2016) or mapping outside of the D1 region (BAC^{T1} (Delpretti et al., 2013) did not display any *lacZ* reporter

247   activity in E12.5 to E13.5 VPs (Fig. 4C). Instead, mouse embryos transgenic for BAC^{Mtx2} (Allais-Bonnet et

248   al., 2021)*,* which covers most of the D1 region, displayed strong reporter expression in the VPs (Fig. 4C).

249   Noteworthy, expression of *Hoxd1* was also abolished from facial mesenchymal progenitors in *Del(attP-SB2)*

250   mouse embryos, while it was reported by X-gal staining of BAC^{Mtx2} transgenic embryos, illustrating that the

251   D1 region regulates the transcription of *Hoxd1* in several tissues.

252   To assess whether the D1 region is also necessary and sufficient for the specific *Hoxd1* expression

253   pattern in somites, we looked at *Hoxd1* transcription in posterior trunk cells using the same set of mutant

254   alleles. *Hoxd1* expression was abolished in developing somites of *Del(attP-SB2)* E9.5 embryos, compared to

255   their control *Del(1-13)* littermates (Fig. 4A, D), while similar transcript levels were maintained in the tailbuds,

256   suggesting that *Hoxd1* regulation in both structures involves different regulatory sequences. Accordingly,

257   embryos transgenic for BAC^{Mtx2} displayed strong lacZ staining in somites but not in the tailbud, with stronger

258   activity in the last formed somites (Fig. 4A, E) thus closely mimicking native *Hoxd1* transcription in these

259   structures (Zákány et al., 2001). In contrast, *lacZ* expression was uniform along the paraxial mesoderm of

260   BAC^{HoxD} transgenic embryos, yet without showing any *Hoxd1*-like specific reporter activity in the forming

261   somites. Altogether, these results confirmed the regulatory potential of the mouse D1 region for *Hoxd1*

262   expression patterns in facial tissues and in forming somites.

263

264   **Emergence of tissue-specific enhancers within conserved chromatin domains.**

265   *Hoxd1* transcription in VPs could have appeared through the evolution of a new CREs, in association

266   with the emergence of these structures in mammals. An alternative possibility would be the re-deployment of

267   a pre-existing element already at work in somites. The latter hypothesis comes from the fact that in both VPs

268   and somites, transcription of *Hoxd1* follows a cyclic dynamic, with a time progression in phase with the

269   production either of somites or of whisker pads. To address this question, we set up to isolate individual VP

270   enhancers and see if they would be active in somites. We generated two smaller BAC transgenes through

271   homologous recombination of a *lacZ* reporter construct, starting from BAC^{Mtx2}. While BAC^{Mtx2a} displayed no

272   signal in VPs, BAC^{Mtx2b} reported stable ß-galactosidase activity (Fig. S4A). Within the BAC^{Mtx2b} region, three

273   candidate enhancers (ECs) were selected based on H3K27ac enrichment, one of them being also H3K27ac-

274   positive in posterior trunk cells (Fig. 4F, black and white arrowheads). Their regulatory potential was assessed

275   using transient *lacZ* reporter assays in transgenic mouse embryos and we identified a strong and reproducible

276   enhancer activity of *tgN^{EC1}* in VPs, comparable to that observed in embryos transgenic for BAC^{Mtx2} (Fig. 4G).

277   Instead, ß-galactosidase activity was not detected neither in *tgN^{EC2}*, nor in *tgN^{EC3}* transgenic embryos (Fig.

278   S4B). We next tested these candidate enhancers at E9.5 to evaluate their regulatory potential in forming

279   somites. *EC2*, which was the only candidate sequence with significant H3K27ac enrichment in posterior trunk

280   cells, displayed reproducible activity in forming somites (Fig. 4H), unlike *tgN^{EC1}* or *tgN^{EC3}* (Fig. S4C). We

281   concluded that the only VP enhancer sequence identified was not active during somite formation, unlike a

282   somite enhancer located nearby (2.7 kb), within the D1 region.

283   The fact that two independent tissue-specific regulations rely on enhancers located in a close proximity

284   within a region of strong interactions suggests that a constrained topology may help the emergence of novel

285   regulatory sequence (Darbellay and Duboule, 2016b). To investigate how CREs might evolve within domains

286   of preferential interactions and how their activity might relate to the observed transcriptional outputs, we

287   compared our mouse and chicken H3K27ac datasets and WISH analyses with the percentage of DNA sequence

288   conservation. The number and distribution of putative CREs (pCREs, defined as non-coding H3K27ac peaks)

289   in the D1, D4 and D9 regions of both mouse and chicken were thus analyzed. Conserved non-coding sequences

290   (CNEs) were annotated by using blastz pairwise alignments downloaded from UCSC and from which all

291   elements overlapping with exons or promoters were discarded (Fig. S4D, E).

292   Overall, the number and distribution of pCREs in the different regions correlated with the

293   transcriptional activity of *Hoxd* genes. A majority of pCRE sequences did not coincide with CNEs, suggesting

294   a lineage-specific evolution of regulatory elements. Amongst those pCREs coinciding with CNEs, several

295   displayed regulatory activities in one species only (Fig. S4, black arrows) indicating a divergence in the

296   combinations of CREs at work, even in posterior trunk cells where the transcriptional activity is expected to

297   be similar in both species. This observation indicates that the sequence conservation of individual regulatory

298   elements is not an obligatory requirement to maintain similar transcription patterns.

299

300   **Divergent enhancer activities of conserved sequences.**

301   To take this analysis genome-wide, we compared the H3K27ac profiles across different mouse and

302   chicken embryonic tissues in relation to the presence of CNEs, by adding available proximal and distal

303   forelimb datasets (Beccari et al., 2016; Yakushiji-Kaminatsui et al., 2018) to our posterior trunk and skin

304   H3K27ac ChIP-seq datasets. pCREs were separated into putative enhancers and promoters, hereafter referred

9

305 to as 'enhancers' and 'promoters' for simplicity, with 'enhancers' mapping more than 2 kb away from a gene

306 transcription start site and 'promoters' mapping less than 2 kb away. pCREs which were H3K27ac-positive in

307 more than one of the analyzed tissues were categorized as 'pleiotropic' while those being active in only one

308 tissue were named 'specific' for the sake of classification. In both mouse and chicken, most promoters were

309 pleiotropic while the majority of enhancers were specific (Fig. 5A), a result in agreement with the usual

310 pleiotropic expression of genes carrying important developmental functions. When enhancers were divided

311 into 'CNEs' or 'non-CNEs', i.e. displaying or not sequence similarities between mouse and chicken, the

312 proportion of pleiotropic enhancers was higher amongst the former (Fig. 5A; p-value < e-15, Fisher test), an

313 increased level of sequence conservation that may reflect the higher evolutionary pressure on enhancers

314 endorsing multiple regulatory functions.

315 　　　Next, we used CNEs to compare the regulatory activities of murine and chicken orthologous

316 sequences. In agreement with what was observed at the *HoxD* locus, the enhancer activities of CNEs, as

317 inferred by H3K27ac peaks, more often diverged than they matched between the related mouse and chicken

318 tissues (Fig. 5B, C). Hierarchical cluster analysis revealed that the enhancer profiles of CNEs were more

319 similar between different tissues of the same species, than between the same tissues in mouse and chicken

320 (Fig. 5B), a surprising observation as these CNEs were initially selected due to their sequence conservation

321 between the two species. We hypothesized that some sequences could have been kept over time despite a

322 divergence in their regulatory activities because they would endorse other functions in other tissues. To

323 evaluate this possibility, we represented on Euler diagrams the relationships between mouse and chicken CNEs

324 displaying enhancer features (Fig. 5C). Each mouse tissue was used as a reference in independent diagrams,

325 where chicken enhancer-CNEs were represented as different sets depending on whether they were active in

326 the same or in different tissues when compared to the mouse reference.

327 　　　The intersection between the same tissue in mouse and in chicken represents elements that have both

328 a conserved sequence and regulatory function (Fig. 5C, overlaps circled in black). This intersection is smaller

329 than any difference between two sets, which indicates that DNA sequence similarity between two species can

330 be maintained amongst regulatory sequences despite divergences in their regulatory functions. We could

331 observe that CNEs often display enhancer activities in a chicken tissue that is different from the mouse tissue,

332 supporting this conclusion (Fig. 5C, overlaps circled in white). As a consequence, the regulatory activity of a

333 given sequence conserved between these two species cannot be used to predict its function(s) in the two

334 species.

335 　　　Altogether, we show that both the global genomic organisation of the <u>*HoxD*</u> locus and specific domains

336 of preferential enhancer-promoter interactions are highly conserved between mouse and chicken. However,

337 the regulatory activities of individual CREs are largely species-specific and such sequences are systematically

338 found within those segments of regulatory landscapes that preferentially interact with the promoters of the

339 most highly transcribed genes. We also show that the lineage-specific evolution of regulatory activities could

340 either generate new regulatory relationships or, conversely, maintain ancestral transcription patterns.

10

341

342 **DISCUSSION**

343 **Versatile *Hoxd* gene functions in skin appendages.**

344   *Hox* genes play a dual role in skin appendage development. While their colinear expression is initially

345 necessary to pattern the skin dermis (Kanzler et al., 1997), they are subsequently transcribed in the dermal

346 papillae and/or ectoderm of embryonic and adult hair pelage follicles and vibrissae precursors (Godwin and

347 Capecchi, 1998; Packer et al., 2000; Reynolds et al., 1995; Yu et al., 2018), as well as in the avian buds

348 (Chuong et al., 1990; Kanzler et al., 1997). Here we show that the dermal papillae of embryonic mouse

349 vibrissae express *Hoxd1* to *Hoxd4*, with the former gene's mRNAs being the first detected, followed by

350 considerably lower levels of *Hoxd3* and *Hoxd4* RNAs. The transcription in VPs is driven by CREs located in

351 a region encompassing approximately 120kb of DNA adjacent to the telomeric end of the mouse *HoxD* cluster,

352 a region that is preferentially contacted by the *Hoxd1* gene. Therefore, a proximity effect is observed in the

353 building of a general chromatin architecture, based on constitutive contacts between the *Hoxd1* region and the

354 neighboring sub-TAD, whereby most of the *Hoxd1* regulatory sequences are located in the adjacent portion of

355 the regulatory landscape.

356   While a detailed functional characterization of *Hoxd* genes during the development of whiskers was

357 not the aim of this work, we did not observe any major morphological alteration in the vibrissae of mice

358 carrying genetic deletions of this precise region, despite the complete abrogation in the expression of *Hoxd1*

359 to *Hoxd4* in these structures. This lack of any visible abnormal phenotype may be due to functional redundancy

360 with other *Hox* paralogy groups expressed there, such as *Hoxc8* (Yu et al., 2018), to a lack of analytical power

361 or of the appropriate behavioral paradigms that may have revealed functionally abnormal whiskers. The

362 diverse expression of *Hox* paralogs in mammalian and avian skin appendages nonetheless illustrates the

363 plasticity in the usage of *Hox* gene functions in these structures. This plasticity likely relies upon the

364 independent acquisition of specific CREs for each gene cluster, as these skin derivatives emerged after the

365 genome duplication events thought to be at the origin of the vertebrate lineage (Holland et al., 2008; Holland

366 and Garcia-Fernàndez, 1996).

367   While *Hoxd9, Hoxd11* and *Hoxd13* are expressed in the ectoderm-derived hair fibers (Godwin and

368 Capecchi, 1998; Packer et al., 2000; Reynolds et al., 1995; Yu et al., 2018), we did not observe any *Hoxd1* in

369 the vibrissae shaft, nor any lacZ activity when the TgBAC[Mtx2] (carrying the D1 region) transgenics were used,

370 indicating that these expression patterns may depend on different sets of CREs. Our data also show that the

371 expression of *Hoxd3* to *Hoxd9* in the ectoderm of the chicken FPs depends on CREs unrelated to those

372 operating in the mouse VPs. These observations may indicate that different sets of *Hoxd* genes were

373 independently co-opted during the evolution of skin derivatives, likely through *de novo* enhancer acquisition

374 in the mammalian and avian lineages, in a way related to the regulation of *Hoxd9 and Hoxc13* in the embryonic

375 mammary buds and in the nails and hairs of mammals, respectively (Fernandez-Guerrero et al., 2020; Schep

376 et al., 2016). Alternatively, the rapid pace of tegument evolution in tetrapods may have been accompanied by

11

377   a divergence in enhancer sequences, which makes comparisons difficult. In this context, we can not rule out

378   the possibility that *Hoxd* gene regulation in skin appendages of both mammals and birds derives from an initial

379   pan-*Hoxd* expression pattern both in the ectoderm and mesoderm of skin appendages, which then evolved

380   differently in each lineage through modification of the CRE complement located within the adjacent TAD.

381   The fact that two CNEs acetylated in mouse VPs and chick FPs are also acetylated in mouse and chick posterior

382   trunk cells may indicate that the former structures co-opted parts of the regulatory mechanisms at work in the

383   latter. In this view, DNA sequence conservation may be due to constraints imposed by the function in the trunk

384   rather than by the function in the skin.

385

386   **Enhancer acquisition in evolving tetrapod skin appendages.**

387   TADs containing pleiotropic genes of key importance for vertebrate development are frequently

388   conserved across tetrapods and topological changes in their organization often correlate with important

389   modifications in gene expression (Eres et al., 2019; Liao et al., 2021; Torosin et al., 2020; Yakushiji-

390   Kaminatsui et al., 2018). Our results show that despite a considerable divergence in the non-coding elements

391   localized in the mouse and chicken T-DOM, the global pattern of interactions is conserved leading to similar

392   chromatin topologies. Indeed, in both cases, different *Hoxd* genes interact preferentially with distinct portions

393   of sub-TAD1. These contacts are for the most constitutive, even though we observed an activity-dependent

394   increase in interactions in the mouse VPs, and in mouse and chicken posterior trunk cells. Of interest, the

395   regions within T-DOM, which were preferentially contacted by the *Hoxd1*, *Hoxd4* or *Hoxd9* genes (D1 to D9)

396   are organized in a linear sequence opposite to the order of the genes themselves, as if *Hoxd1* was folding on

397   its closest possible chromatin environment within T-DOM, bringing along *Hoxd3* towards the next chromatin

398   segment and positioning the interactions involving *Hoxd9* further away into T-DOM. This sequential

399   positioning of interactions in mirror with spatial colinearity may impose a generic contact pattern, whereby

400   *Hoxd9*, for example, is unable to establish strong interactions with the D1 region and its enhancers, for this

401   region is primarily contacting *Hoxd1*, thus imposing constraints upon the distributions of interactions (see

402   below).

403   Furthermore, the distribution of H3K27ac-positive regions in the chicken FPs and mouse VPs across

404   these interacting regions correlate well with the specific subsets of *Hoxd* genes expressed in each of these

405   tissues. Finally, the regulation of *Hoxd1* in developing somites relies on evolutionary conserved elements

406   located in the region D1. This general regulatory topology is close to that observed in teleost fishes (Acemel

407   et al., 2016; Woltering et al., 2014), suggesting that it was already in place at the root of the vertebrate lineage

408   and that its hijacking by nascent enhancer sequences, may have favoured the co-option of specific *Hoxd* gene

409   subsets as targets of the novel regulations. The regulation of *Hoxd* genes in the mouse VPs and chicken FPs,

410   as well in the mouse mammary buds (Schep et al., 2016) may illustrate this process.

411

412   **Plasticity of the *cis*-regulatory code *versus* conservation in TAD organization.**

12

413   Due to their functional relevance in the regulation of gene expression, CREs tend to be evolutionarily

414   conserved across species (Sandelin et al., 2004; Sanges et al., 2013, 2006). However, several studies have

415   shown that enhancers controlling developmental gene expression can be functionally conserved even across

416   distant phylogenetic lineages despite a strong divergence in their DNA sequences (Ambrosino et al., 2019;

417   Berthelot et al., 2018; Wong et al., 2020) (Eichenlaub and Ettwiller, 2011; Schmidt et al., 2010; Villar et al.,

418   2015). Our inter-species comparison of CNEs enriched in H3K27ac across different embryonic structures

419   revealed that a considerable portion of evolutionary conserved CREs diverged in their patterns of activity

420   between the two species analyzed, in agreement with previous observations (Dermitzakis and Clark, 2002;

421   Schmidt et al., 2010; Vierstra et al., 2014; Villar et al., 2015). This dichotomy between the conservation of

422   enhancer sequences and their function is illustrated by the CREs controlling *Hoxd1* expression in the mouse

423   and chicken developing somites. While some of the sequences active in the mouse posterior trunk are

424   evolutionary and functionally conserved in chicken, such as EC2, which can drive lacZ expression in the last

425   formed somites of the murine embryo, other elements conserved at the nucleotide level displayed H3K27ac

426   enrichment only in the mouse.

427   In fact, a large fraction of H3K27ac-positive sequences detected either in the mouse or in the chicken

428   posterior trunk cells were not conserved between the two species, suggesting that they evolved in a species-

429   specific manner. In contrast, the high proportion of chicken promoters that display similar H3K27ac

430   enrichments in mice, together with the similar expression patterns observed for mouse and chicken *Hoxd* genes

431   in embryonic trunk cells, demonstrate that conserved gene expression can occur despite a high evolutionary

432   plasticity in the *cis*-regulatory code usage, in agreement with previous reports (Berthelot et al., 2018; Snetkova

433   et al., 2021). This may point to a regulatory strategy where multiple enhancers act coordinately to regulate the

434   same target gene(s) thus creating a quantitative effect in a way similar to the reported action of super-enhancers

435   (Sabari et al., 2018), yet where various subsets of CREs may display distinct tissue-specificities. This process

436   may be implemented preferentially within large regulatory landscapes, as e.g. in the case of *Fgf8* (Marinic et

437   al., 2013) or the TAD controlling *Hoxd* gene transcription in external genitals (Amândio et al., 2020).

438

A regulatory playground with constraints.

439

440   In those cases that were investigated, the respective positions of regulatory sequences within large

441   syntenic regulatory landscapes are generally conserved, and the global regulatory architecture found at one

442   particular developmental locus in one species can be extrapolated to its cognate locus in another amniote

443   species (e.g. (Kragesteen et al., 2018), implying that enhancer-promoter interactions are also evolutionary well

444   conserved, even for CREs acting over long distances (Irimia et al., 2012; Laverré et al., 2021), although some

445   mechanistic elements may vary (Ushiki et al., 2021). In agreement with this, and contrasting with the apparent

446   divergence in the *cis*-regulatory code controlling *Hoxd* gene expression in mouse and chicken embryos, our

447   phylogenetic footprinting and epigenetic analysis revealed that non-coding elements conserved in their DNA

448   sequence between the mouse and chicken genomes were distributed across the two species in a very similar

13

449   manner. Therefore, the potential gain and/or loss in the two lineages of particular CREs did not significantly

450   impact the internal organization of those conserved regulatory elements, nor did they impact upon the global

451   chromatin topology of the locus. This confirms the observation that even the significant divergence in CREs

452   located at the *HoxD* locus, which accompanied the evolution of the snake body plan, did not result in any

453   substantial alteration of the overall corn-snake *Hoxd* gene interaction map (Guerreiro et al., 2016). Altogether,

454   these observations suggest that the internal organization of the TADs at the *HoxD* locus and the specific

455   interaction profiles for various subsets of *Hoxd* target genes are resilient to considerable variation in their

456   CREs.

457   These results also highlight the somewhat dual properties that large regulatory landscapes may have

458   imposed in the course of regulatory evolution. On the one hand, a pre-established chromatin topology, as

459   materialized by TADs, may have provided unique 'structural niches' to evolve new enhancer sequences, due

460   to the proximity of factors already at work. This might especially apply to landscapes where a strong

461   quantitative parameter may be instrumental, and *a fortiori* when the target gene(s) are acting in combination,

462   coding for proteins of rather low specificities (Bolt and Duboule, 2020). This may be illustrated nowadays by

463   large landscapes, where all kinds of enhancer sequences are mixed within the same TAD. On the other hand,

464   this regulatory playground, while stimulating the emergence of regulations, will constrain their realms of action

465   due both to the very architecture that favors their evolution and to the accessibility to 'a' subset of contiguous

466   target genes as a result of the global distribution of interactions at this precise place of the landscape.

467

468   **MATERIAL AND METHODS**

469   **Mouse strains and chicken eggs**

470   All mutant strains are listed in Table S1 and were backcrossed continuously to Bl6/CBA mixed animals and

471   maintained as heterozygous stocks. Chick embryos from a White Leghorn strain were incubated at 37.5°C and

472   staged according to Hamburger and Hamilton (1951).

473   **Enhancer cloning and transgenic animals**

474   The different CRE candidate sequences were amplified using PCR-specific primers (see Table S2) and the

475   Expand High Fidelity PCR system (Roche). Amplified fragments were gel-purified and cloned into the pSK-

476   lacZ vector as in (Beccari et al., 2016). For the transgenesis assays, each lacZ reporter construct was digested

477   with NotI and KpnI and the restriction fragment encoding the potential enhancer sequence, the beta-globin

478   minimal promoter and the lacZ reporter gene was gel-purified and injected into the male pronucleus of

479   fertilized oocytes. F0 embryos were dissected either at E10, or at E12, fixed and stained for lacZ activity

480   according to standard protocols.

481   ***In situ* hybridization**

482   The probes used in this study for *in situ* hybridization were either previously reported, or produced by PCR

483   amplification of a fragment subsequently ligated in pGEMT Easy vector (Promega). Primers used to amplify

14

484   the fragment of interest are listed in Table S2. Digoxigenin (Dig) labeled probes were synthesized *in vitro* by

485   linearizing the respective plasmids using specific restriction enzymes and transcribed *in vitro* either with

486   T7/T3, or Sp6 RNA polymerase (Table S3) and the Dig-RNA labeling mix (Roche). The probes were purified

487   using the RNA easy mini kit. WISH experiments were performed as described in (Woltering et al., 2009).

488   Probes are listed in (Table S3). *In situ* experiments in sections were performed according to (Sockanathan and

489   Sockanathan, 2015). Cryostat sections were prepared after fixing embryos in 4% PFA solution at 4ºC

490   overnight. Subsequently, embryos were washed three times with PBS and passed to increasing sucrose

491   solutions at 4ºC in agitation (15% sucrose solution for 3-4 hours, followed by incubation in 30% sucrose

492   solution overnight) and finally included in OCT blocks. Sections of 20 μm were obtained with a Leica cryostat

493   and stored at -80ºC.

494   **ChIP-seq**

495   For genomics analyses, we used the mouse assembly mm10 and the chicken galGal6 and we plotted genomic

496   data with pyGenomeTracks 3.6 (Lopez-Delisle et al., 2021). ChIP-seq experiments were performed using the

497   ChIP-IT High sensitivity kit (active motif according to manufacturer instructions with minor modifications).

498   For the mouse samples, 12 pairs of E12.5 WPs, or one hundred E8.75 posterior trunks were used, the latter

499   dissected at the level of the 2nd to 4th pair of somites. For the chicken samples, the dorsal skin of five HH35

500   embryos or the posterior trunk or 80 HH19-21 posterior trunk regions were isolated. In all cases, the samples

501   were fixed for 10 min in 1% formaldehyde at RT and the crosslinking reaction was quenched with Glycine.

502   Subsequently, nuclei were extracted and sonicated in (Tris HCl pH 8.0 50mM, EDTA 10mM, 1% SDS) to

503   an average fragment size of 200-500bp using a Diagenonode Bioruptor Sonicator. Ca. 10 to 20 μg of sonicated

504   chromatin were diluted tenfold with Dilution buffer (HEPES pH 7.3 20mM, EDTA 1mM, NaCl 150mM, NP40

505   0.1%) and incubated with 2 μg of anti-H3K27ac antibody (Abcam, ab4729). All buffers contained 1X

506   Complete Proteinase Inhibitor cocktail (EDTA-free; Roche) and 10mM Sodium Butyrate to prevent protein

507   degradation and Histone de-acetylation. Chromatin–antibody complexes were immunoprecipitated with

508   Protein G-coupled agarose beads-purified and de-crosslinked according to manufacturer instructions. Approx

509   5 to 10 ng of purified DNA were used for ChIP library preparation by the Geneva IGE3 Genomics Platform

510   (University of Geneva) and sequenced to obtain 100-bp single-end reads on an Illumina HiSeq2500 or

511   HiSeq4000 system. Published fastq files were downloaded from SRA for H3K27ac: mouse DFL

512   (GSM2713703, SRR5855214), mouse PFL (GSM2713704, SRR5855215), chicken DFL (GSM3182462,

513   SRR7288104), chicken PFL (GSM3182459, SRR7288101); and for CTCF in mouse PT (GSM5501395,

514   SRR15338248). ChIP-seq reads processing was done as in (Amândio et al., 2020) with some modifications,

515   using the laboratory Galaxy server (Afgan et al., 2016). Adapters and bad-quality bases were removed with

516   Cutadapt (v1.16.8) (Martin, 2011) (options -m 15 -q 30 -a

517   GATCGGAAGAGCACACGTCTGAACTCCAGTCAC). Reads were mapped to the mouse genome

518   (mm10) and to the chicken genome (galGla6) using Bowtie2 (v2.4.2) (Langmead and Salzberg, 2012)

519   with standard settings. Only alignments with a mapping quality >30 were kept (Samtools v1.13) (Danecek et

15

520 al. 2021). H3K27ac ChIP mapped reads were down sampled with Samtools view (v1.13) according to the

521 sample with the smallest number of reads after filtering and duplicate removal (mouse: 71741225 reads;

522 chicken 25872853 reads). Mouse CTCF ChIP mapped reads were down sampled with a fraction of 1/4 and

523 chicken CTCF ChIP reads were not down sampled. When two replicates were available, alignment bam files

524 were merged with Samtools merge (v1.13) and subsampled to the same number as single replicates. The

525 coverage and peaks were obtained as the output of MACS2 (v2.1.1.20160309.6) (Zhang et al., 2008) with a

526 fixed extension of 200 bp (--call-summits --nomodel --extsize 200 -B), and, for the WP sample, the q-value

527 cutoff for peak detection was set to 0.1 instead of the 0.05 default. CTCF motif orientation was assessed using

528 peaks extended by 100 bp each side and the CTCFBSDB 2.0 database (Ziebarth et al., 2012) with MIT_LM7

529 identified motifs.

530 **MAR annotation**

531 MARs are genomic segments of the T-DOM with the highest density of specific H3K27ac coverage and are

532 annotated as follow: For mm10 chr2:74872605-75696338 and for galGal6 chr7:15856252-16252401, sliding

533 windows are of 10 kb every 2 kb. For each window the coverage of the ChIP was computed and the difference

534 with the coverage in the corresponding H3K27ac ChIP in the brain was considered as the specific signal. The

535 smallest sequence of consecutive windows cumulating 30% (for the DS and WP samples) or 50% (for the PT

536 samples) of the total specific signal is the MAR. See ChIP_scanRegionForHighestDensity_2files.py at

537 https://gitlab.unige.ch/Aurelie.Hintermann/hintermannetal2022 for all details.

538 **pCREs**

539 pCREs are defined as genomic intervals that overlap with H3K27ac Macs2 peaks in at least one of the samples

540 analyzed per species. To obtain the genomic coordinates of pCREs, Macs2 peaks of all samples were pooled

541 into one file, the size of each peak was increased by 660 bp each side to account for nucleosome occupancy

542 with bedtools slop (v2.30.0), and overlapping Macs2 peaks were combined into a single pCRE interval using

543 bedtools merge. pCREs were annotated according to their colocalization with tissue-specific H3K27ac peaks,

544 exons and sequence conservation using bedtools intersect. pCREs were quantified using R (v3.6.1) and the bar

545 plots of Figure 5A were done with the ggplot2 package (v3.2.1). See CNEs_01.sh at

546 https://gitlab.unige.ch/Aurelie.Hintermann/hintermannetal2022 for all details.

547 **CNEs**

548 Pairwise blastz alignments were downloaded from

549 http://hgdownload.soe.ucsc.edu/goldenPath/mm10/vsGalGal6/mm10.galGal6.synNet.maf.gz and

550 transformed to intervals with maf to interval (Blankenberg et al., 2011). Conserved elements were considered

551 non-coding if they would not overlap with annotated exons neither in mouse nor in chicken. The synteny plot

552 on Figure S3A was done using the R package ggplot2 (v3.2.1). CNEs were annotated according to their

553 colocalization with tissue-specific H3K27ac peaks, exons and sequence conservation using bedtools intersect.

554 pCREs were quantified using R (v3.6.1) and the bar plots of Figure 5A were done with the ggplot2 package

555 (v3.2.1) (R Core Team (2019). R: A language and environment for statistical computing. R Foundation for

16

556 Statistical Computing, Vienna, Austria. URL https://www.R-project.org/.). The heatmap in Figure 5B was

557 done using the pheatmap R package (v1.0.12) using a matrix which columns are CNEs that overlapped with

558 an enhancer in at least one tissue in mouse or in chicken, rows are the tissues in which acetylation peaks were

559 called and values are the scores of acetylation peaks. If a CNE comprised several peaks of the same tissue, the

560 average was done. In Figure 5C, the relationships of the three sets formed by the conditions of being acetylated

561 in the mouse tissue, in the chicken tissue or in a chicken tissue excepted the one considered were represented

562 on Euler diagramms using the eulerr R package (v6.0.0), considering independently each tissue analyzed (i.e.

563 PT DFL PFL Skin and FB). See CNEs_01.sh at

564 https://gitlab.unige.ch/Aurelie.Hintermann/hintermannetal2022 for all details.

565 **4C-seq experiments**

566 4C-seq experiments were performed according to (Noordermeer et al., 2011). Briefly, the tissues were

567 dissected, dissociated with collagenase (Sigma Aldrich/Fluka) and filtered through a 35 microns mesh. Cells

568 were fixed with 2% formaldehyde (in PBS/10%FBS) for 10 min at RT and the reaction was quenched on ice

569 with Glycine. Nuclei were extracted using a cell lysis buffer (Tris pH 7.5 10 mM, NaCl 10 mM, MgCl$_2$ 5 mM,

570 EDTA 0.1 mM,) and stored at -80°C. Approximately 200 E9.5 posterior trunk regions dissected at the level of

571 the 2nd to 4th pair of somites, as well as 120 chicken HH19-21 posterior trunk samples, were used. Nuclei were

572 digested with NlaIII (New England Biolabs) and ligated with T4 DNA ligase HC (Promega) in diluted

573 conditions to promote intramolecular ligation. Samples were digested again with DpnII (New England

574 Biolabs) and re-ligated with T4 DNA ligase HC. These templates were amplified using Expand long template

575 (Roche) and PCR barcoded primers flanked with adaptors. For each library, 8 to 10 independent PCR reactions

576 were pooled together and purified using the PCR purification kit (Qiagen). Multiplexed libraries were

577 sequenced on Illumina HiSeq 2500 to obtain 100 bp single-end reads. Demultiplexing, mapping and 4C-seq

578 analysis were performed using a local version of the pipeline described in (David et al., 2014), on the mouse

579 mm10 and chicken galGal6 genome assemblies. The profiles were smoothened using a window size of 11

580 fragments and normalized to the mean score in +/-5 Mb around the viewpoint. When multiple independent

581 biological replicates were available, average 4C-seq profiles were calculated. When viewpoints were

582 subtracted, the score of each window of the normalized, smoothed profiles were subtracted (See

583 4C_subset_subtract at https://gitlab.unige.ch/Aurelie.Hintermann/hintermannetal2022) for all details.

584 **Capture Hi-C-seq experiments**

585 The SureSelectXT RNA probe design and capture Hi-C experiments were performed as described in (Bolt et

586 al., 2021b) for mouse and as in (Yakushiji-Kaminatsui et al., 2018) for chicken. Dissected tissues were

587 processed as in (Yakushiji-Kaminatsui et al., 2018) with the following changes: cells were cross-linked in 2%

588 formaldehyde/PBS and washed three times instead of being quenched by glycine. Hi-C-libraries were prepared

589 as in (Yakushiji-Kaminatsui et al., 2018). The first part of the data analysis was performed on our local galaxy

590 server (Afgan et al. 2016). Raw reads were preprocessed with CutAdapt (v1.16) (-a

591 AGATCGGAAGAGCACACGTCTGAACTCCAGTCAC   -A

17

592 AGATCGGAAGAGCGTCGTGTAGGGAAAGAGTGTAGATCTCGGTGGTCGCCGTATCATT --

593 minimum-length=15 --pair-filter=any --quality-cutoff=30) (Martin 2011). Then, Hicup (v0.6.1) (Langmead

594 and Salzberg 2012; Dryden et al. 2014) and Samtools 1.2 (Danecek et al. 2021) were used with default

595 parameters. The pairs were then loaded to 5-kb (mouse) and 2.5-kb (chicken) resolution matrices with Cooler

596 v0.7.4 (Abdennur and Mirny 2020). These matrices were balanced with HiCExplorer hicCorrectMatrix

597 (v3.7.2) using ICE as correction method, the mad threshold from HiCExplorer hicCorrectMatrix diagnostic

598 plot as minimum threshold value and 5 as maximum threshold value. The TAD separation scores were

599 computed with HiCExplorer hicFindTADs. (Ramírez et al. 2018; Wolff et al. 2020) with a fixed window of

600 240 kb in the mouse and 120 kb in the chicken. See CHiC_processRaws.sh

601 https://gitlab.unige.ch/Aurelie.Hintermann/hintermannetal2022 for all details.

602

ETHICS APPROVAL

604 All experiments involving animals were performed in agreement with the Swiss Law on Animal Protection

605 (LPA), under license No GE 81/14 (to DD).

DATA AVAILABILITY

607 All raw and processed datasets are available in the Gene Expression Omnibus (GEO) repository under

608 accession number GSE195592. All scripts necessary to reproduce figures from raw data are available at

609 https://gitlab.unige.ch/Aurelie.Hintermann/hintermannetal2022.

COMPETING INTERESTS

611 The authors declare that they have no competing interests.

FUNDING

AUTHORS CONTRIBUTIONS

618 A. H. : Designed experiments, realized experiments and interpreted the results, wrote the manuscript

619 I. G. : Did some cloning and *in situ* hybridizations

620 C. C. B. : Provided unpublished datasets and helped for some the CHi-C experiments

621 L. L.-D.: Helped with the bioinformatic analyses

622 S. G. : Genotyped and helped analyze mouse mutants.

18

623   D. D. : Designed experiments, interpreted some results and wrote the paper.

624   L. B. : Designed experiments, interpreted some results and wrote the paper.

631

632   **LEGENDS TO FIGURES**

633   **Figure 1. Transcription of *Hoxd* genes in mammalian and avian skin primordia. A.** Schematic illustration

634   of a E12.5 mouse embryo with VPs (Vibrissae Primordia) represented as red circles. The dorso-ventral (D-V)

635   and the caudo-rostral (C-R) axes are shown as red arrows representing the timing of appearance of the vibrissae

636   primordia. **B.** WISH on E12.5 faces. The arrowheads point to the most caudo-dorsal placode, which is the

637   largest one and the first to appear. Staining intensity progressively decreases from *Hoxd1* to *Hoxd8*. **C.**

638   Schematic illustration of the back of a HH35 chicken embryo with feather placodes as red circles. A, anterior;

639   P, posterior. **D.** WISH on HH35 chicken showing the skin of the upper back. The arrowheads point to the neck

640   at the level of the shoulders. *HOXD1* is not expressed, whereas *HOXD3* and *HOXD8* signal intensities are

641   stronger than for *HOXD4* and *HOXD9*. **E.** Schematic representation of a E9.5 or HH20 posterior trunk and

642   tailbud. A, anterior; P, posterior; PSM, presomitic mesoderm; NT*,* neural tube; IM, intermediate mesoderm;

643   FS, forming somites; PM, paraxial mesoderm; LM, lateral mesoderm; S*,* somites. **F.** WISH on E9.5 mouse

644   posterior trunk and tail bud. *Hoxd1* transcription pattern is different from that of *Hoxd4* and *Hoxd9*. **G.** WISH

645   on HH20 chicken posterior trunk and tail bud. *HOXD1* transcription pattern is different from *HOXD4* and

646   *HOXD9*. The white arrowheads in panels **F** and **G** point to the *Hoxd1* stripe in the PSM. The black arrowheads

647   show the difference between mouse (**F**) and chicken (**G**) in the *Hoxd1* mRNAs persistence in formed somites.

648

649   **Figure 2. Capture Hi-C-seq at the mouse and chicken *HoxD* loci. A**, **B.** Capture Hi-C-seq heatmaps using

650   dissected posterior trunk cells. Below each heatmap, a CTCF ChIP-seq track is shown, produced from the

651   same material. The similarities in the structural organization of the mouse and the chicken loci are underlined

652   either by the positions of syntenic CNEs at key positions (numbered vertical dashed lines), the domains

653   produced by TAD calling (black bars below) and the presence of a sub-TAD boundary (asterisk) within T-

654   DOM. Genes are represented by empty rectangles. In panel **A,** E9.5 mouse posterior trunk cells were used and

655   the CHi-C heatmap was mapped on mm10 with a bin size of 5 kb (chr2:73800000-75800000). In panel **B,**

656   HH20 chicken posterior trunk cells were used and the CHi-C heatmap mapped on galGal6 with a bin size of

657   2.5kb (chr7:15790000-16700000) and on an inverted x-axis. The positions of the two TADs (T-DOM and C-

658   DOM) and of both sub-TADs are shown on top. The scales on the X axes were adjusted to comparable sizes

659   for ease of comparison, yet the chicken locus is more compacted (see the scale bars, bottom right).

660

661   **Figure 3. Tissue- and gene-specific interactions of dense H3K27ac regions. A.** On top is a ChIP-seq profile

662   of H3K27ac using mouse E12.5 VPs (orange) superimposed over the E12.5 forebrain cells (grey) (mm10,

663   chr2:73800000-75800000). Below is a H3K27ac profile produced from dissected chicken HH35 dorsal skin

664   (green), with HH18 brain cells (grey)(galGal6, chr7:15790000-16700000, inverted x-axis). The highest

665   interacting regions are depicted as D1, D4 and D9 (see also Figure S3B). The positions of conserved CNEs

666   were used to delimit these regions in both species (vertical dashed lines) and the extents of TADs are shown

667   below (thick black lines). The T-DOM (empty red rectangle) is split in overlapping genomic windows and the

668   densest window (Most Acetylated Region; MAR) is shown as a filled red rectangle. In the mouse VP, the

669   MAR is within the D1 DNA segment, whereas the chicken MAR overlaps with the D4 and D9 regions. **B.**

670   H3K27ac ChIP-seq using mouse E9.5 posterior trunk cells (orange) superimposed over forebrain cells

671   (grey)(mm10, chr2:73800000-75800000). Below is shown the H3K27ac profile obtained from the same

672   sample but dissected from a HH18 chicken embryo (green) with brain cells (grey) as a control (galGal6,

673   chr7:15790000-16700000, inverted x-axis). While the mouse posterior trunk Most Acetylated Region (MAR,

674   red rectangle) coincides with the D4 segment, the chicken MAR counterpart also covers D4 and a small part

675   of D9.

676

677   **Figure 4. Transcriptional regulation of *Hoxd1*. A.** The three deletion lines used are shown in red lines and

678   the transgenic BACs in blue lines. The extent of the D1 to D9 regions are shown on top (black) as well as the

679   positions of both sub-TADs below (thick black lines). **B.** WISH using a *Hoxd1* probe on E12.5 mouse embryos.

680   *Hoxd1* mRNAs were detected in both the control and the Del(SB2-SB3) lines (red arrowheads), yet the signal

681   was absent from Del(attP-SB2) mutant embryos (white arrowheads). **C.** X-gal staining on E12.5 mouse

682   embryos carrying randomly integrated BACs. A strong staining was detected in VPs when BAC^{Mtx2} was used

683   (red arrowhead), whereas staining was not scored with the other two flanking BAC clones (white arrowheads).

684   Therefore, a region directly downstream the *HoxD* cluster is necessary and sufficient to activate *Hoxd1*

685   transcription in VPs, referred to as D1 region as it coincides with this previously defined region. **D.** WISH of

686   *Hoxd1* on E9.5 embryos focusing on tail buds. *Hoxd1* was detected in forming somites in both the control and

687   the *Del(SB2-SB3)* lines (red arrowheads), but was absent from *Del(attP-SB2)* mutant embryos (white

688   arrowhead). **E.** X-gal staining of E9.5 mouse embryos carrying various BAC transgenes. Staining was scored

689   in the entire neural tube and paraxial mesoderm with the BAC^{HoxD} (black arrowhead). In contrast, embryos

690   carrying BAC^{Mtx2} displayed staining in forming somites (red arrowhead), a staining absent when BAC^{T1} was

691   used (white arrowhead). **F.** Enlargement of the D1 region along with a H3K27ac ChIP-seq using dissected

692   E12.5 VPs (orange, top) and E9.5 posterior trunk cells (orange, bottom) superimposed over E12.5 forebrain

20

693   (FB) cells (grey) (mm10; chr2:74747751-74916570). Above the profiles are the three VP acetylated elements

694   (black arrowheads) and below are MACS2 narrowPeaks for VPs and PTs (orange) and FB (grey). The position

695   of the three EC sequences used as transgenes (tgEC) are shown by numbered black boxes. **G.** X-gal staining

696   in VPs on a E12.5 embryo transgenic for *EC1*. **H.** X-gal staining in forming somites on E9.5 embryo transgenic

697   for the *EC2* sequence.

698

699   **Figure 5. Conserved sequences with divergent functions. A.** Bar plots showing the proportion of putative

700   *cis*-regulatory elements (pCREs) harbouring the H3K27ac mark in one ('specific') *versus* more than one

701   ('pleiotropic') tissues, in either mouse (orange) or chicken (green). For simplification purposes, distal pCREs

702   (>2kb away from the transcription start site) are referred as 'enhancers' and proximal pCREs (<2kb away from

703   transcription start site) are called 'promoters'. The different proportions are shown when comparing enhancers

704   and promoters (left), and conserved enhancers to non-conserved enhancers (right). The proportion of specific

705   *versus* pleiotropic elements is shown for CNEs and non-CNEs enhancers (right). In both mouse and chicken,

706   enhancers are more specific than promoters and amongst enhancers, conserved elements are found acetylated

707   in more tissues than non-conserved elements. **B.** Hierarchical clustering obtained using pheatmap R package.

708   On the *X*-axis are shown enhancer-CNEs i.e., conserved sequences, which are non-coding in mouse and in

709   chicken and which overlap with a H3K27ac mark in at least one species. On the *Y*-axis are displayed those

710   tissues used to obtain MACS2 processed peaks. The values on the heatmap correspond to the enrichment

711   scores of the peaks. Enhancer-CNEs cluster by species and not by tissues. **C.** Euler diagrams representing the

712   proportion of enhancer-CNEs, per tissue, acetylated in mouse (orange), in the corresponding chicken tissue

713   (dark green), or in unrelated chicken tissue (light green), showing that conserved sequence diverge in their

714   regulatory activities. The intersection between the same tissue in mouse and in chicken is delineated by a black

715   line, and the intersection between a chicken tissue different from the mouse tissue is delineated by a white line.

716   In **B.** and **C.** PFL, proximal forelimb; DFL, distal forelimb; posterior trunk, posterior trunk; DS, dorsal skin.

717

718   **LEGENDS TO SUPPLEMENTARY FIGURES**

719

720   **Supplementary Figure S1. Evolution of the *HoxD* locus and expression of *Hoxd* genes in the developing**

721   **VPs. A.** On the left is a schematic illustration of a vertebrate phylogenetic tree showing the emergence of some

722   skin derivatives (glands, scales, feathers, hairs). On the right are the corresponding versions of the *HoxD* locus,

723   with the orthologous *HoxD* gene clusters as shaded orange areas and other orthologous genes shown in green

724   to help delimit the extent of the conserved regulatory landscapes. **B.** Schematic representation of vibrissae

725   morphogenesis: epithelial placode (EP, yellow cells); dermal condensation (DC, blue cells). The approximate

726   developmental stage is indicated below, showing the delay between vibrissae and hair morphogenesis. The

727   dorsal skin of the upper back was used as reference for hairs. **C.** WISH on three successive E12 staged embryos

728   (indicated on the left) using four *Hoxd* genes as probes (top). The same three placodes are pointed by red

21

729   (positive) or white (negative) arrowheads. **D.** Schematic of the transversal section on E13.5 VPs (left),

730   analyzed in ISH with a *Hoxd1* probe (right). The scale bar in the right picture corresponds to 100 μm and the

731   *Hoxd1* stained VPs at peg stage (see below) are indicated by red arrowheads of decreasing intensities from left

732   to right. The staining is localized in dermal cells. **E.** WISH on E12.5 bisected mouse embryos. *Hoxd1* mRNAs

733   were detected after those for *Shh* (left) and before *Hoxd4* mRNAs (right).

734

735   **Supplementary Figure S2. Feather development and transcription of *Hoxd* genes. A.** Schematic of feather

736   development between stage HH20 and HH35 with ectodermal placode (EP, yellow) and dermal condensation

737   cells (DC, blue). **B.** WISH on HH35 chicken embryos, dorsal view of the upper back, with arrowheads pointing

738   toward the neck at the shoulder level. *HOXD11* transcripts were not detected in FPs (right), unlike those of

739   SHH (left). **C.** Transversal section through a HH35 chicken skin of the upper back (red), corresponding to the

740   two sections stained by ISH on the right. The scale bar is 100 μm. *SHH* is used as marker of the epithelial

741   placode (red arrowhead). *HOXD8* is also transcribed in epithelial placodes, matching -or slightly larger than-

742   the *SHH* domain.

743

744   **Supplementary Figure S3. Comparative 4C-seq analyses at the mouse and chicken *HoxD* loci. A.** Synteny

745   plots representing sequences conserved between the mouse and the chicken *HoxD* loci. On the X-axis is the

746   mouse locus (mm10, chr2:73800000-75800000) and on the Y axis is the chicken locus (galGal6,

747   chr7:15790000-16700000, inverted x-axis). The scale is the same for both axes. TADs and sub-TADs are

748   indicated by black lines and the *HoxD* cluster by a red rectangle. Schematic representations of the locus are on

749   top of each axis. Despite a mouse locus that is in average 2.2 times larger than its chicken counterpart, the

750   order of the conserved sequences is maintained, showing the absence of substantial genomic rearrangement at

751   this locus. **B.** On the Y axis are 4C-seq normalised scores per feature, with E9.5 mouse posterior trunk cells

752   scores (orange) superimposed over E12.5 FB cells (grey). Below the 4C tracks, the positions of the *Hoxd1,*

753   *Hoxd4* and *Hoxd9* viewpoints are represented by triangles, with a black triangle for the viewpoint used in the

754   track. Between each track, the subtraction of the two adjacent viewpoints is represented (black). The

755   preferentially interacting regions D1, D4 and D9 were annotated manually and, to facilitate comparisons

756   between their positions in the mouse and the chicken locus, orthologous CNEs located close to the edge of

757   each region D are shown (vertical dashed lines). CTCF ChIP-seq profiles are displayed below the 4C tracks,

758   with red and blue arrowheads below indicating their orientation. Color intensity is proportional to motif score.

759   Data mapped on mm10, chr2:73800000-75800000. **C.** On the Y axis are 4C-seq normalised scores per feature,

760   using HH18 chicken posterior trunk cells (green), superimposed with the profile obtained with HH18 brain

761   cells (grey). Data shown for *HOXD1* (top) *HOXD4* (middle) and *HOXD9* (bottom) viewpoints, with a black

762   arrowhead indicating the position of the viewpoint. Reads mapped on galGal6, chr7:15790000-16700000,

763   inverted x-axis.

22

Supplementary Figure S4. Comparison of conserved and non-conserved CREs in mouse and chicken embryonic tissues. A. X-gal staining of E12.5 transgenic embryos carrying either the first half (left) or the second half (right) of *BAC^Mtx2*. The entire *BAC^Mtx2* recapitulated the pattern of expression of *Hoxd1* in VPs. **B.** Staining of embryos carrying either the *TgN^EC2* or the *TgN^EC3* transgenes, which show no regulatory activity in VPs at E12.5. **C.** Staining of E9.5 mouse embryos carrying the *TgN^EC1* or the *TgN^EC3* reporter constructs, which show the absence of signal in forming somites. **D.** H3K27ac ChIP-seq profiles magnifications over the mouse and chicken sub-TAD1. Top: Mouse E12.5 dissected VPs (orange) along with the mouse E12.5 forebrain cells track (grey)(mm10, chr2:74775737-75222876). Below is the profile for the chicken HH35 dorsal skin (green), superimposed to HH18 brain cells (grey) (galGal6, chr7:16033612-16252401, inverted x-axis). Processed MACS2 narrowPeaks are in orange/green vertical lines and blastz conserved sequences in black vertical lines, below each track. The peaks overlapping CNEs are pointed by black arrows. The peaks corresponding to CNEs in both species and in equivalent tissues are pointed by red arrows. Vertical dashed lines represent the position of corresponding CNEs at the edge of each region **E.** H3K27ac ChIP-seq focusing on sub-TAD1. Top: The profile for mouse E9.5 posterior trunk cells (orange) are superimposed to mouse E12.5 forebrain cells (grey). Bottom: Profiles of chicken HH18 embryonic posterior trunk cells (green) and of HH18 brain cells.

LEGENDS TO SUPPLEMENTARY TABLES

Supplementary Table S1. List of mouse lines

Supplementary Table S2. Primers used to clone candidate enhancer sequences

Supplementary Table S3. Probes for *in situ* hybridization

788

BIBLIOGRAPHY

789

790 Acemel, R.D., Tena, J.J., Irastorza-Azcarate, I., Marlétaz, F., Gómez-Marín, C., de la Calle-
791 Mustienes, E., Bertrand, S., Diaz, S.G., Aldea, D., Aury, J.-M., Mangenot, S., Holland, P.W.H.,
792 Devos, D.P., Maeso, I., Escrivá, H., Gómez-Skarmeta, J.L., 2016. A single three-dimensional
793 chromatin compartment in amphioxus indicates a stepwise evolution of vertebrate Hox bimodal
794 regulation. Nat. Genet. 48, 336–341. https://doi.org/10.1038/ng.3497
795 Afgan, E., Baker, D., van den Beek, M., Blankenberg, D., Bouvier, D., Čech, M., Chilton, J.,
796 Clements, D., Coraor, N., Eberhard, C., Grüning, B., Guerler, A., Hillman-Jackson, J., Von Kuster,
797 G., Rasche, E., Soranzo, N., Turaga, N., Taylor, J., Nekrutenko, A., Goecks, J., 2016. The Galaxy
798 platform for accessible, reproducible and collaborative biomedical analyses: 2016 update. Nucleic
799 Acids Res. 44, W3–W10. https://doi.org/10.1093/nar/gkw343
800 Allais-Bonnet, A., Hintermann, A., Deloche, M.-C., Cornette, R., Bardou, P., Naval-Sanchez, M.,
801 Pinton, A., Haruda, A., Grohs, C., Zakany, J., Bigi, D., Medugorac, I., Putelat, O., Greyvenstein, O.,
802 Hadfield, T., Jemaa, S.B., Bunevski, G., Menzi, F., Hirter, N., Paris, J.M., Hedges, J., Palhiere, I.,
803 Rupp, R., Lenstra, J.A., Gidney, L., Lesur, J., Schafberg, R., Stache, M., Wandhammer, M.-D.,
804 Arbogast, R.-M., Guintard, C., Blin, A., Boukadiri, A., Rivière, J., Esquerré, D., Donnadieu, C.,
805 Danchin-Burge, C., Reich, C.M., Riley, D.G., Marle-Koster, E. van, Cockett, N., Hayes, B.J.,
806 Drögemüller, C., Kijas, J., Pailhoux, E., Tosser-Klopp, G., Duboule, D., Capitan, A., 2021.
807 Analysis of Polycerate Mutants Reveals the Evolutionary Co-option of *HOXD1* for Horn Patterning
808 in Bovidae. Mol. Biol. Evol. 38, 2260–2272. https://doi.org/10.1093/molbev/msab021
809 Amândio, A.R., Lopez-Delisle, L., Bolt, C.C., Mascrez, B., Duboule, D., 2020. A complex
810 regulatory landscape involved in the development of mammalian external genitals. eLife 9, e52962.
811 https://doi.org/10.7554/eLife.52962
812 Ambrosino, L., Vassalli, Q.A., D'Agostino, Y., Esposito, R., Cetrangolo, V., Caputi, L., Amoroso,
813 A., Aniello, F., D'Aniello, S., Chatzigeorgiou, M., Chiusano, M.L., Locascio, A., 2019. Functional
814 conserved non-coding elements among tunicates and chordates. Dev. Biol., Current Directions in
815 Tunicate Development 448, 101–110. https://doi.org/10.1016/j.ydbio.2018.12.012
816 Andrey, G., Montavon, T., Mascrez, B., Gonzalez, F., Noordermeer, D., Leleu, M., Trono, D.,
817 Spitz, F., Duboule, D., 2013. A switch between topological domains underlies HoxD genes
818 collinearity in mouse limbs. Science 340, 1234167. https://doi.org/10.1126/science.1234167
819 Beccari, L., Yakushiji-Kaminatsui, N., Woltering, J.M., Necsulea, A., Lonfat, N., Rodriguez-
820 Carballo, E., Mascrez, B., Yamamoto, S., Kuroiwa, A., Duboule, D., 2016. A role for HOX13
821 proteins in the regulatory switch between TADs at the HoxD locus. Genes Dev. 30, 1172–1186.
822 https://doi.org/10.1101/gad.281055.116
823 Belton, J.-M., McCord, R.P., Gibcus, J., Naumova, N., Zhan, Y., Dekker, J., 2012. Hi-C: A
824 comprehensive technique to capture the conformation of genomes. Methods San Diego Calif 58.
825 https://doi.org/10.1016/j.ymeth.2012.05.001
826 Berthelot, C., Villar, D., Horvath, J.E., Odom, D.T., Flicek, P., 2018. Complexity and conservation
827 of regulatory landscapes underlie evolutionary resilience of mammalian gene expression. Nat. Ecol.
828 Evol. 2, 152–163. https://doi.org/10.1038/s41559-017-0377-2
829 Biggs, L.C., Mikkola, M.L., 2014. Early inductive events in ectodermal appendage morphogenesis.
830 Blankenberg, D., Taylor, J., Nekrutenko, A., 2011. Making whole genome multiple alignments
831 usable for biologists. Bioinformatics 27, 2426–2428. https://doi.org/10.1093/bioinformatics/btr398
832 Bolt, C.C., Duboule, D., 2020. The regulatory landscapes of developmental genes. Development
833 147, dev171736. https://doi.org/10.1242/dev.171736
834 Bolt, C.C., Lopez-Delisle, L., Mascrez, B., Duboule, D., 2021a. Mesomelic dysplasias associated
835 with the HOXD locus are caused by regulatory reallocations. Nat. Commun. 12, 5013.
836 https://doi.org/10.1038/s41467-021-25330-y

24

837 Bolt, C.C., Lopez-Delisle, L., Mascrez, B., Duboule, D., 2021b. MESOMELIC DYSPLASIAS
838 ASSOCIATED WITH THE HOXD LOCUS ARE CAUSED BY REGULATORY
839 REALLOCATIONS. bioRxiv 2021.02.01.429171. https://doi.org/10.1101/2021.02.01.429171
840 Bompadre, O., Andrey, G., 2019. Chromatin topology in development and disease. Curr. Opin.
841 Genet. Dev. 55, 32–38. https://doi.org/10.1016/j.gde.2019.04.007
842 Carroll, S.B., 2008. Evo-Devo and an Expanding Evolutionary Synthesis: A Genetic Theory of
843 Morphological Evolution. Cell 134, 25–36. https://doi.org/10.1016/j.cell.2008.06.030
844 Chiang, C., Swan, R.Z., Grachtchouk, M., Bolinger, M., Litingtung, Y., Robertson, E.K., Cooper,
845 M.K., Gaffield, W., Westphal, H., Beachy, P.A., Dlugosz, A.A., 1999. Essential role for Sonic
846 hedgehog during hair follicle morphogenesis. Dev. Biol. 205, 1–9.
847 https://doi.org/10.1006/dbio.1998.9103
848 Chuong, C.M., Oliver, G., Ting, S.A., Jegalian, B.G., Chen, H.M., De Robertis, E.M., 1990.
849 Gradients of homeoproteins in developing feather buds. Dev. Camb. Engl. 110, 1021–1030.
850 Creyghton, M.P., Cheng, A.W., Welstead, G.G., Kooistra, T., Carey, B.W., Steine, E.J., Hanna, J.,
851 Lodato, M.A., Frampton, G.M., Sharp, P.A., Boyer, L.A., Young, R.A., Jaenisch, R., 2010. Histone
852 H3K27ac separates active from poised enhancers and predicts developmental state. Proc Natl Acad
853 Sci USA 107, 21931–21936. https://doi.org/10.1073/pnas.1016071107
854 Dale, K.J., Pourquié, O., 2000. A clock-work somite. BioEssays 22, 72–83.
855 https://doi.org/10.1002/(SICI)1521-1878(200001)22:1<72::AID-BIES12>3.0.CO;2-S
856 Darbellay, F., Bochaton, C., Lopez-Delisle, L., Mascrez, B., Tschopp, P., Delpretti, S., Zakany, J.,
857 Duboule, D., 2019. The constrained architecture of mammalian Hox gene clusters. Proc. Natl.
858 Acad. Sci. U. S. A. 116, 13424–13433. https://doi.org/10.1073/pnas.1904602116
859 Darbellay, F., Duboule, D., 2016a. Chapter Sixteen - Topological Domains, Metagenes, and the
860 Emergence of Pleiotropic Regulations at Hox Loci, in: Wassarman, P.M. (Ed.), Current Topics in
861 Developmental Biology, Essays on Developmental Biology, Part A. Academic Press, pp. 299–314.
862 Darbellay, F., Duboule, D., 2016b. Topological Domains, Metagenes, and the Emergence of
863 Pleiotropic Regulations at Hox Loci. Curr. Top. Dev. Biol. 116, 299–314.
864 https://doi.org/10.1016/bs.ctdb.2015.11.022
865 David, F.P.A., Delafontaine, J., Carat, S., Ross, F.J., Lefebvre, G., Jarosz, Y., Sinclair, L.,
866 Noordermeer, D., Rougemont, J., Leleu, M., 2014. HTSstation: A Web Application and Open-
867 Access Libraries for High-Throughput Sequencing Data Analysis. PLoS ONE 9, e85879.
868 https://doi.org/10.1371/journal.pone.0085879
869 Dekker, J., Heard, E., 2015. Structural and functional diversity of Topologically Associating
870 Domains. FEBS Lett. 589, 2877–2884. https://doi.org/10.1016/j.febslet.2015.08.044
871 Delpretti, S., Montavon, T., Leleu, M., Joye, E., Tzika, A., Milinkovitch, M., Duboule, D., 2013.
872 Multiple enhancers regulate Hoxd genes and the Hotdog LncRNA during cecum budding. Cell Rep.
873 5, 137–50. https://doi.org/10.1016/j.celrep.2013.09.002
874 Dermitzakis, E.T., Clark, A.G., 2002. Evolution of Transcription Factor Binding Sites in
875 Mammalian Gene Regulatory Regions: Conservation and Turnover. Mol. Biol. Evol. 19, 1114–
876 1121. https://doi.org/10.1093/oxfordjournals.molbev.a004169
877 Dhouailly, D., 2009. A new scenario for the evolutionary origin of hair, feather, and avian scales. J.
878 Anat. 214, 587–606. https://doi.org/10.1111/j.1469-7580.2008.01041.x
879 Dhouailly, D., Godefroit, P., Martin, T., Nonchev, S., Caraguel, F., Oftedal, O., 2019. Getting to the
880 root of scales, feather and hair: As deep as odontodes? Exp. Dermatol. 28, 503–508.
881 https://doi.org/10.1111/exd.13391
882 Di-Poï, N., Milinkovitch, M.C., 2016. The anatomical placode in reptile scale morphogenesis
883 indicates shared ancestry among skin appendages in amniotes. Sci. Adv. 2, e1600708.
884 https://doi.org/10.1126/sciadv.1600708
885 Dixon, J.R., Selvaraj, S., Yue, F., Kim, A., Li, Y., Shen, Y., Hu, M., Liu, J.S., Ren, B., 2012.

25

886   Topological domains in mammalian genomes identified by analysis of chromatin interactions.
887   Nature 485, 376–380.
888   Edwards, S.L., Beesley, J., French, J.D., Dunning, A.M., 2013. Beyond GWASs: Illuminating the
889   Dark Road from Association to Function. Am. J. Hum. Genet. 93, 779–797.
890   https://doi.org/10.1016/j.ajhg.2013.10.012
891   Eichenlaub, M.P., Ettwiller, L., 2011. De Novo Genesis of Enhancers in Vertebrates. PLoS Biol. 9.
892   https://doi.org/10.1371/journal.pbio.1001188
893   Eres, I.E., Luo, K., Hsiao, C.J., Blake, L.E., Gilad, Y., 2019. Reorganization of 3D genome
894   structure may contribute to gene regulatory evolution in primates. PLOS Genet. 15, e1008278.
895   https://doi.org/10.1371/journal.pgen.1008278
896   Fernandez-Guerrero, M., Yakushiji-Kaminatsui, N., Lopez-Delisle, L., Zdral, S., Darbellay, F.,
897   Perez-Gomez, R., Bolt, C.C., Sanchez-Martin, M.A., Duboule, D., Ros, M.A., 2020. Mammalian-
898   specific ectodermal enhancers control the expression of Hoxc genes in developing nails and hair
899   follicles. Proc. Natl. Acad. Sci. U. S. A. 117, 30509–30519.
900   https://doi.org/10.1073/pnas.2011078117
901   Gaunt, S., Sharpe, P.T., Duboule, D., 1988. Spatially restricted domains of homeo-gene transcripts
902   in mouse embryos: relation to a segmented body plan. Development 104 (suppl), 169–179.
903   Godwin, A.R., Capecchi, M.R., 1998. Hoxc13 mutant mice lack external hair. Genes Dev. 12, 11–
904   20.
905   Guerreiro, I., Gitto, S., Novoa, A., Codourey, J., Nguyen Huynh, T.H., Gonzalez, F., Milinkovitch,
906   M.C., Mallo, M., Duboule, D., 2016. Reorganisation of Hoxd regulatory landscapes during the
907   evolution of a snake-like body plan. eLife 5, e16087. https://doi.org/10.7554/eLife.16087
908   Hamburger, V., Hamilton, H.L., 1951. A series of normal stages in the development of the chick
909   embryo. J. Morphol. 88, 49–92. https://doi.org/10.1002/jmor.1050880104
910   Hansen, A.S., Pustova, I., Cattoglio, C., Tjian, R., Darzacq, X., 2017. CTCF and cohesin regulate
911   chromatin loop stability with distinct dynamics. eLife 6, e25776.
912   https://doi.org/10.7554/eLife.25776
913   Harmston, N., Ing-Simmons, E., Tan, G., Perry, M., Merkenschlager, M., Lenhard, B., 2017.
914   Topologically associating domains are ancient features that coincide with Metazoan clusters of
915   extreme noncoding conservation. Nat. Commun. 8. https://doi.org/10.1038/s41467-017-00524-5
916   Holland, L.Z., Albalat, R., Azumi, K., Benito-Gutiérrez, È., Blow, M.J., Bronner-Fraser, M.,
917   Brunet, F., Butts, T., Candiani, S., Dishaw, L.J., Ferrier, D.E.K., Garcia-Fernàndez, J., Gibson-
918   Brown, J.J., Gissi, C., Godzik, A., Hallböök, F., Hirose, D., Hosomichi, K., Ikuta, T., Inoko, H.,
919   Kasahara, M., Kasamatsu, J., Kawashima, T., Kimura, A., Kobayashi, M., Kozmik, Z., Kubokawa,
920   K., Laudet, V., Litman, G.W., McHardy, A.C., Meulemans, D., Nonaka, M., Olinski, R.P., Pancer,
921   Z., Pennacchio, L.A., Pestarino, M., Rast, J.P., Rigoutsos, I., Robinson-Rechavi, M., Roch, G.,
922   Saiga, H., Sasakura, Y., Satake, M., Satou, Y., Schubert, M., Sherwood, N., Shiina, T., Takatori, N.,
923   Tello, J., Vopalensky, P., Wada, S., Xu, A., Ye, Y., Yoshida, K., Yoshizaki, F., Yu, J.-K., Zhang,
924   Q., Zmasek, C.M., Jong, P.J. de, Osoegawa, K., Putnam, N.H., Rokhsar, D.S., Satoh, N., Holland,
925   P.W.H., 2008. The amphioxus genome illuminates vertebrate origins and cephalochordate biology.
926   Genome Res. 18, 1100–1111. https://doi.org/10.1101/gr.073676.107
927   Holland, P.W.H., Garcia-Fernàndez, J., 1996. HoxGenes and Chordate Evolution. Dev. Biol. 173,
928   382–395. https://doi.org/10.1006/dbio.1996.0034
929   Irimia, M., Tena, J.J., Alexis, M.S., Fernandez-Miñan, A., Maeso, I., Bogdanovic, O., de la Calle-
930   Mustienes, E., Roy, S.W., Gómez-Skarmeta, J.L., Fraser, H.B., 2012. Extensive conservation of
931   ancient microsynteny across metazoans due to cis-regulatory constraints. Genome Res. 22, 2356–
932   2367. https://doi.org/10.1101/gr.139725.112
933   Kanzler, B., Prin, F., Thelu, J., Dhouailly, D., 1997. CHOXC-8 and CHOXD-13 expression in
934   embryonic chick skin and cutaneous appendage specification. Dev. Dyn. Off. Publ. Am. Assoc.

26

935 Anat. 210, 274–287. https://doi.org/10.1002/(SICI)1097-0177(199711)210:3<274::AID-
936 AJA8>3.0.CO;2-D
937 Kanzler, B., Viallet, J.P., Le Mouellic, H., Boncinelli, E., Duboule, D., Dhouailly, D., 1994.
938 Differential expression of two different homeobox gene families during mouse tegument
939 morphogenesis. Int. J. Dev. Biol. 38, 633–640.
940 Kragesteen, B.K., Spielmann, M., Paliou, C., Heinrich, V., Schöpflin, R., Esposito, A.,
941 Annunziatella, C., Bianco, S., Chiariello, A.M., Jerković, I., Harabula, I., Guckelberger, P.,
942 Pechstein, M., Wittler, L., Chan, W.-L., Franke, M., Lupiáñez, D.G., Kraft, K., Timmermann, B.,
943 Vingron, M., Visel, A., Nicodemi, M., Mundlos, S., Andrey, G., 2018. Dynamic 3D chromatin
944 architecture contributes to enhancer specificity and limb morphogenesis. Nat. Genet. 50, 1463–
945 1473. https://doi.org/10.1038/s41588-018-0221-x
946 Langmead, B., Salzberg, S.L., 2012. Fast gapped-read alignment with Bowtie 2. Nat Methods 9,
947 357–9. https://doi.org/10.1038/nmeth.1923
948 Laverré, A., Tannier, E., Necsulea, A., 2021. Long-range promoter-enhancer contacts are conserved
949 during evolution and contribute to gene expression robustness. bioRxiv 2021.02.26.432473.
950 https://doi.org/10.1101/2021.02.26.432473
951 Liao, Y., Zhang, X., Chakraborty, M., Emerson, J.J., 2021. Topologically associating domains and
952 their role in the evolution of genome structure and function in Drosophila. Genome Res. 31, 397–
953 410. https://doi.org/10.1101/gr.266130.120
954 Long, H.K., Prescott, S.L., Wysocka, J., 2016. Ever-Changing Landscapes: Transcriptional
955 Enhancers in Development and Evolution. Cell 167, 1170–1187.
956 https://doi.org/10.1016/j.cell.2016.09.018
957 Lopez-Delisle, L., Rabbani, L., Wolff, J., Bhardwaj, V., Backofen, R., Grüning, B., Ramírez, F.,
958 Manke, T., 2021. pyGenomeTracks: reproducible plots for multivariate genomic datasets.
959 Bioinformatics 37, 422–423. https://doi.org/10.1093/bioinformatics/btaa692
960 Lupianez, D.G., Kraft, K., Heinrich, V., Krawitz, P., Brancati, F., Klopocki, E., Horn, D., Kayserili,
961 H., Opitz, J.M., Laxova, R., Santos-Simarro, F., Gilbert-Dussardier, B., Wittler, L., Borschiwer, M.,
962 Haas, S.A., Osterwalder, M., Franke, M., Timmermann, B., Hecht, J., Spielmann, M., Visel, A.,
963 Mundlos, S., 2015. Disruptions of topological chromatin domains cause pathogenic rewiring of
964 gene-enhancer interactions. Cell 161, 1012–25. https://doi.org/10.1016/j.cell.2015.04.004
965 Marinic, M., Aktas, T., Ruf, S., Spitz, F., 2013. An integrated holo-enhancer unit defines tissue and
966 gene specificity of the Fgf8 regulatory landscape. Dev. Cell 24, 530–42.
967 https://doi.org/10.1016/j.devcel.2013.01.025
968 Martin, M., 2011. Cutadapt removes adapter sequences from high-throughput sequencing reads.
969 EMBnet.journal 17. https://doi.org/10.14806/ej.17.1.200
970 Michon, F., Charveron, M., Dhouailly, D., 2007. Dermal condensation formation in the chick
971 embryo: Requirement for integrin engagement and subsequent stabilization by a possible
972 Notch/integrin interaction. Dev. Dyn. 236, 755–768. https://doi.org/10.1002/dvdy.21080
973 Mikkola, M.L., 2007. Genetic basis of skin appendage development. Semin. Cell Dev. Biol.,
974 Mechanisms and biological significance of RNA localization AND Development of ectodermal
975 appendages 18, 225–236. https://doi.org/10.1016/j.semcdb.2007.01.007
976 Montavon, T., Soshnikova, N., Mascrez, B., Joye, E., Thevenet, L., Splinter, E., de Laat, W., Spitz,
977 F., Duboule, D., 2011. A Regulatory Archipelago Controls Hox Genes Transcription in Digits. Cell
978 147, 1132–1145. https://doi.org/10.1016/j.cell.2011.10.023
979 Nanni, L., Ceri, S., Logie, C., 2020. Spatial patterns of CTCF sites define the anatomy of TADs and
980 their boundaries. Genome Biol. 21, 197. https://doi.org/10.1186/s13059-020-02108-x
981 Noordermeer, D., Leleu, M., Splinter, E., Rougemont, J., De Laat, W., Duboule, D., 2011. The
982 dynamic architecture of Hox gene clusters. Science 334, 222–5.
983 https://doi.org/10.1126/science.1207194

984 Nora, E.P., Lajoie, B.R., Schulz, E.G., Giorgetti, L., Okamoto, I., Servant, N., Piolot, T., van
985 Berkum, N.L., Meisig, J., Sedat, J., Gribnau, J., Barillot, E., Bluthgen, N., Dekker, J., Heard, E.,
986 2012. Spatial partitioning of the regulatory landscape of the X-inactivation centre. Nature 485, 381–
987 5. https://doi.org/10.1038/nature11049
988 Packer, A.I., Jane-wit, D., McLean, L., Panteleyev, A.A., Christiano, A.M., Wolgemuth, D.J., 2000.
989 Hoxa4 expression in developing mouse hair follicles and skin. Mech. Dev. 99, 153–157.
990 https://doi.org/10.1016/S0925-4773(00)00471-8
991 Pantalacci, S., Chaumot, A., Benoît, G., Sadier, A., Delsuc, F., Douzery, E.J.P., Laudet, V., 2008.
992 Conserved features and evolutionary shifts of the EDA signaling pathway involved in vertebrate
993 skin appendage development. Mol. Biol. Evol. 25, 912–928.
994 https://doi.org/10.1093/molbev/msn038
995 Pugacheva, E.M., Kubo, N., Loukinov, D., Tajmul, M., Kang, S., Kovalchuk, A.L., Strunnikov,
996 A.V., Zentner, G.E., Ren, B., Lobanenkov, V.V., 2020. CTCF mediates chromatin looping via N-
997 terminal domain-dependent cohesin retention. Proc. Natl. Acad. Sci. U. S. A. 117, 2020–2031.
998 https://doi.org/10.1073/pnas.1911708117
999 Rada-Iglesias, A., Bajpai, R., Swigut, T., Brugmann, S.A., Flynn, R.A., Wysocka, J., 2011. A
1000 unique chromatin signature uncovers early developmental enhancers in humans. Nature 470, 279–
1001 283. https://doi.org/10.1038/nature09692
1002 Rao, S.S.P., Huntley, M.H., Durand, N.C., Stamenova, E.K., Bochkov, I.D., Robinson, J.T.,
1003 Sanborn, A.L., Machol, I., Omer, A.D., Lander, E.S., Aiden, E.L., 2014. A 3D Map of the Human
1004 Genome at Kilobase Resolution Reveals Principles of Chromatin Looping. Cell 159, 1665–1680.
1005 https://doi.org/10.1016/j.cell.2014.11.021
1006 Rebeiz, M., Patel, N.H., Hinman, V.F., 2015. Unraveling the Tangled Skein: The Evolution of
1007 Transcriptional Regulatory Networks in Development. Annu. Rev. Genomics Hum. Genet. 16, 103–
1008 131. https://doi.org/10.1146/annurev-genom-091212-153423
1009 Reid, A.I., Gaunt, S.J., 2002. Colinearity and non-colinearity in the expression of Hox genes in
1010 developing chick skin. Int. J. Dev. Biol. 46, 209–15. https://doi.org/10.1387/ijdb.011495
1011 Reynolds, A.J., Lawrence, C.M., Jahoda, C.A., 1995. Hair follicle and fiber reconstruction. J.
1012 Invest. Dermatol. 104, 39S-40S. https://doi.org/10.1038/jid.1995.57
1013 Rodríguez-Carballo, E., Lopez-Delisle, L., Willemin, A., Beccari, L., Gitto, S., Mascrez, B.,
1014 Duboule, D., 2020. Chromatin topology and the timing of enhancer function at the HoxD locus.
1015 Proc. Natl. Acad. Sci. U. S. A. 117, 31231–31241. https://doi.org/10.1073/pnas.2015083117
1016 Rodriguez-Carballo, E., Lopez-Delisle, L., Zhan, Y., Fabre, P.J., Beccari, L., El-Idrissi, I., Huynh,
1017 T.H.N., Ozadam, H., Dekker, J., Duboule, D., 2017. The HoxD cluster is a dynamic and resilient
1018 TAD boundary controlling the segregation of antagonistic regulatory landscapes. Genes Dev. 31,
1019 2264–2281. https://doi.org/10.1101/gad.307769.117
1020 Sabari, B.R., Dall'Agnese, A., Boija, A., Klein, I.A., Coffey, E.L., Shrinivas, K., Abraham, B.J.,
1021 Hannett, N.M., Zamudio, A.V., Manteiga, J.C., Li, C.H., Guo, Y.E., Day, D.S., Schuijers, J., Vasile,
1022 E., Malik, S., Hnisz, D., Lee, T.I., Cisse, I.I., Roeder, R.G., Sharp, P.A., Chakraborty, A.K., Young,
1023 R.A., 2018. Coactivator condensation at super-enhancers links phase separation and gene control.
1024 Science 361. https://doi.org/10.1126/science.aar3958
1025 Sandelin, A., Bailey, P., Bruce, S., Engström, P.G., Klos, J.M., Wasserman, W.W., Ericson, J.,
1026 Lenhard, B., 2004. Arrays of ultraconserved non-coding regions span the loci of key developmental
1027 genes in vertebrate genomes. BMC Genomics 5, 99. https://doi.org/10.1186/1471-2164-5-99
1028 Sanges, R., Hadzhiev, Y., Gueroult-Bellone, M., Roure, A., Ferg, M., Meola, N., Amore, G., Basu,
1029 S., Brown, E.R., De Simone, M., Petrera, F., Licastro, D., Strähle, U., Banfi, S., Lemaire, P.,
1030 Birney, E., Müller, F., Stupka, E., 2013. Highly conserved elements discovered in vertebrates are
1031 present in non-syntenic loci of tunicates, act as enhancers and can be transcribed during
1032 development. Nucleic Acids Res. 41, 3600–3618. https://doi.org/10.1093/nar/gkt030

1033   Sanges, R., Kalmar, E., Claudiani, P., D'Amato, M., Muller, F., Stupka, E., 2006. Shuffling of cis-
1034   regulatory elements is a pervasive feature of the vertebrate lineage. Genome Biol. 7, R56.
1035   https://doi.org/10.1186/gb-2006-7-7-r56
1036   Sawyer, R.H., Knapp, L.W., 2003. Avian skin development and the evolutionary origin of feathers.
1037   J. Exp. Zoolog. B Mol. Dev. Evol. 298, 57–72. https://doi.org/10.1002/jez.b.26
1038   Schep, R., Necsulea, A., Rodríguez-Carballo, E., Guerreiro, I., Andrey, G., Nguyen Huynh, T.H.,
1039   Marcet, V., Zákány, J., Duboule, D., Beccari, L., 2016. Control of Hoxd gene transcription in the
1040   mammary bud by hijacking a preexisting regulatory landscape. Proc. Natl. Acad. Sci. U. S. A. 113,
1041   E7720–E7729. https://doi.org/10.1073/pnas.1617141113
1042   Schmidt, D., Wilson, M.D., Ballester, B., Schwalie, P.C., Brown, G.D., Marshall, A., Kutter, C.,
1043   Watt, S., Martinez-Jimenez, C.P., Mackay, S., Talianidis, I., Flicek, P., Odom, D.T., 2010. Five-
1044   Vertebrate ChIP-seq Reveals the Evolutionary Dynamics of Transcription Factor Binding. Science
1045   328, 1036–1040. https://doi.org/10.1126/science.1186176
1046   Sexton, T., Yaffe, E., Kenigsberg, E., Bantignies, F., Leblanc, B., Hoichman, M., Parrinello, H.,
1047   Tanay, A., Cavalli, G., 2012. Three-dimensional folding and functional organization principles of
1048   the Drosophila genome. Cell 148, 458–72. https://doi.org/10.1016/j.cell.2012.01.010
1049   Snetkova, V., Ypsilanti, A.R., Akiyama, J.A., Mannion, B.J., Plajzer-Frick, I., Novak, C.S.,
1050   Harrington, A.N., Pham, Q.T., Kato, M., Zhu, Y., Godoy, J., Meky, E., Hunter, R.D., Shi, M.,
1051   Kvon, E.Z., Afzal, V., Tran, S., Rubenstein, J.L.R., Visel, A., Pennacchio, L.A., Dickel, D.E., 2021.
1052   Ultraconserved enhancer function does not require perfect sequence conservation. Nat. Genet. 53,
1053   521–528. https://doi.org/10.1038/s41588-021-00812-3
1054   Sockanathan, S., Sockanathan, S., 2015. In situ hybridization of chick and mouse embryonic tissue.
1055   Protoc. Exch. https://doi.org/10.1038/protex.2015.040
1056   Spitz, F., Furlong, E.E.M., 2012. Transcription factors: from enhancer binding to developmental
1057   control. Nat. Rev. Genet. 13, 613–626. https://doi.org/10.1038/nrg3207
1058   Spitz, F., Gonzalez, F., Peichel, C., Vogt, T.F., Duboule, D., Zakany, J., 2001. Large scale
1059   transgenic and cluster deletion analysis of the HoxD complex separate an ancestral regulatory
1060   module from evolutionary innovations. Genes Dev 15, 2209–14.
1061   https://doi.org/10.1101/gad.205701
1062   Torosin, N.S., Anand, A., Golla, T.R., Cao, W., Ellison, C.E., 2020. 3D genome evolution and
1063   reorganization in the Drosophila melanogaster species group. PLOS Genet. 16, e1009229.
1064   https://doi.org/10.1371/journal.pgen.1009229
1065   Ushiki, A., Zhang, Y., Xiong, C., Zhao, J., Georgakopoulos-Soares, I., Kane, L., Jamieson, K.,
1066   Bamshad, M.J., Nickerson, D.A., University of Washington Center for Mendelian Genomics, Shen,
1067   Y., Lettice, L.A., Silveira-Lucas, E.L., Petit, F., Ahituv, N., 2021. Deletion of CTCF sites in the
1068   SHH locus alters enhancer-promoter interactions and leads to acheiropodia. Nat. Commun. 12,
1069   2282. https://doi.org/10.1038/s41467-021-22470-z
1070   Vierstra, J., Rynes, E., Sandstrom, R., Zhang, M., Canfield, T., Hansen, R.S., Stehling-Sun, S.,
1071   Sabo, P.J., Byron, R., Humbert, R., Thurman, R.E., Johnson, A.K., Vong, S., Lee, K., Bates, D.,
1072   Neri, F., Diegel, M., Giste, E., Haugen, E., Dunn, D., Wilken, M.S., Josefowicz, S., Samstein, R.,
1073   Chang, K.-H., Eichler, E.E., De Bruijn, M., Reh, T.A., Skoultchi, A., Rudensky, A., Orkin, S.H.,
1074   Papayannopoulou, T., Treuting, P.M., Selleri, L., Kaul, R., Groudine, M., Bender, M.A.,
1075   Stamatoyannopoulos, J.A., 2014. Mouse regulatory DNA landscapes reveal global principles of cis-
1076   regulatory evolution. Science 346, 1007–1012. https://doi.org/10.1126/science.1246426
1077   Villar, D., Berthelot, C., Aldridge, S., Rayner, T.F., Lukk, M., Pignatelli, M., Park, T.J., Deaville,
1078   R., Erichsen, J.T., Jasinska, A.J., Turner, J.M.A., Bertelsen, M.F., Murchison, E.P., Flicek, P.,
1079   Odom, D.T., 2015. Enhancer Evolution across 20 Mammalian Species. Cell 160, 554–566.
1080   https://doi.org/10.1016/j.cell.2015.01.006
1081   Widelitz, R.B., Chuong, C.M., 1999. Early events in skin appendage formation: induction of

1082   epithelial placodes and condensation of dermal mesenchyme. J. Investig. Dermatol. Symp. Proc.
1083   Soc. Investig. Dermatol. Inc Eur. Soc. Dermatol. Res. 4, 302–306.
1084   https://doi.org/10.1038/sj.jidsp.5640234
1085   Woltering, J.M., Noordermeer, D., Leleu, M., Duboule, D., 2014. Conservation and Divergence of
1086   Regulatory Strategies at Hox Loci and the Origin of Tetrapod Digits. PLoS Biol 12, e1001773.
1087   https://doi.org/10.1371/journal.pbio.1001773
1088   Wong, E.S., Zheng, D., Tan, S.Z., Bower, N.I., Garside, V., Vanwalleghem, G., Gaiti, F., Scott, E.,
1089   Hogan, B.M., Kikuchi, K., McGlinn, E., Francois, M., Degnan, B.M., 2020. Deep conservation of
1090   the enhancer regulatory code in animals. Science 370. https://doi.org/10.1126/science.aax8137
1091   Wu, P., Hou, L., Plikus, M., Hughes, M., Scehnet, J., Suksaweang, S., Widelitz, R., Jiang, T.-X.,
1092   Chuong, C.-M., 2004. Evo-Devo of amniote integuments and appendages. Int. J. Dev. Biol. 48,
1093   249–270. https://doi.org/10.1387/ijdb.041825pw
1094   Yakushiji-Kaminatsui, N., Lopez-Delisle, L., Bolt, C.C., Andrey, G., Beccari, L., Duboule, D.,
1095   2018. Similarities and differences in the regulation of HoxD genes during chick and mouse limb
1096   development. PLoS Biol. 16, e3000004. https://doi.org/10.1371/journal.pbio.3000004
1097   Yu, Z., Jiang, K., Xu, Z., Huang, H., Qian, N., Lu, Z., Chen, D., Di, R., Yuan, T., Du, Z., Xie, W.,
1098   Lu, X., Li, H., Chai, R., Yang, Y., Zhu, B., Kunieda, T., Wang, F., Chen, T., 2018. Hoxc-
1099   Dependent Mesenchymal Niche Heterogeneity Drives Regional Hair Follicle Regeneration. Cell
1100   Stem Cell 23, 487-500.e6. https://doi.org/10.1016/j.stem.2018.07.016
1101   Zákány, J., Kmita, M., Alarcon, P., de la Pompa, J.-L., Duboule, D., 2001. Localized and Transient
1102   Transcription of Hox Genes Suggests a Link between Patterning and the Segmentation Clock. Cell
1103   106, 207–217. https://doi.org/10.1016/S0092-8674(01)00436-6
1104   Zhang, Y., Liu, T., Meyer, C.A., Eeckhoute, J., Johnson, D.S., Bernstein, B.E., Nusbaum, C.,
1105   Myers, R.M., Brown, M., Li, W., Liu, X.S., 2008. Model-based analysis of ChIP-Seq (MACS).
1106   Genome Biol 9, R137. https://doi.org/10.1186/gb-2008-9-9-r137
1107   Ziebarth, J.D., Bhattacharya, A., Cui, Y., 2012. CTCFBSDB 2.0: a database for CTCF-binding sites
1108   and genome organization. Nucleic Acids Res. 41, D188–D194. https://doi.org/10.1093/nar/gks1165
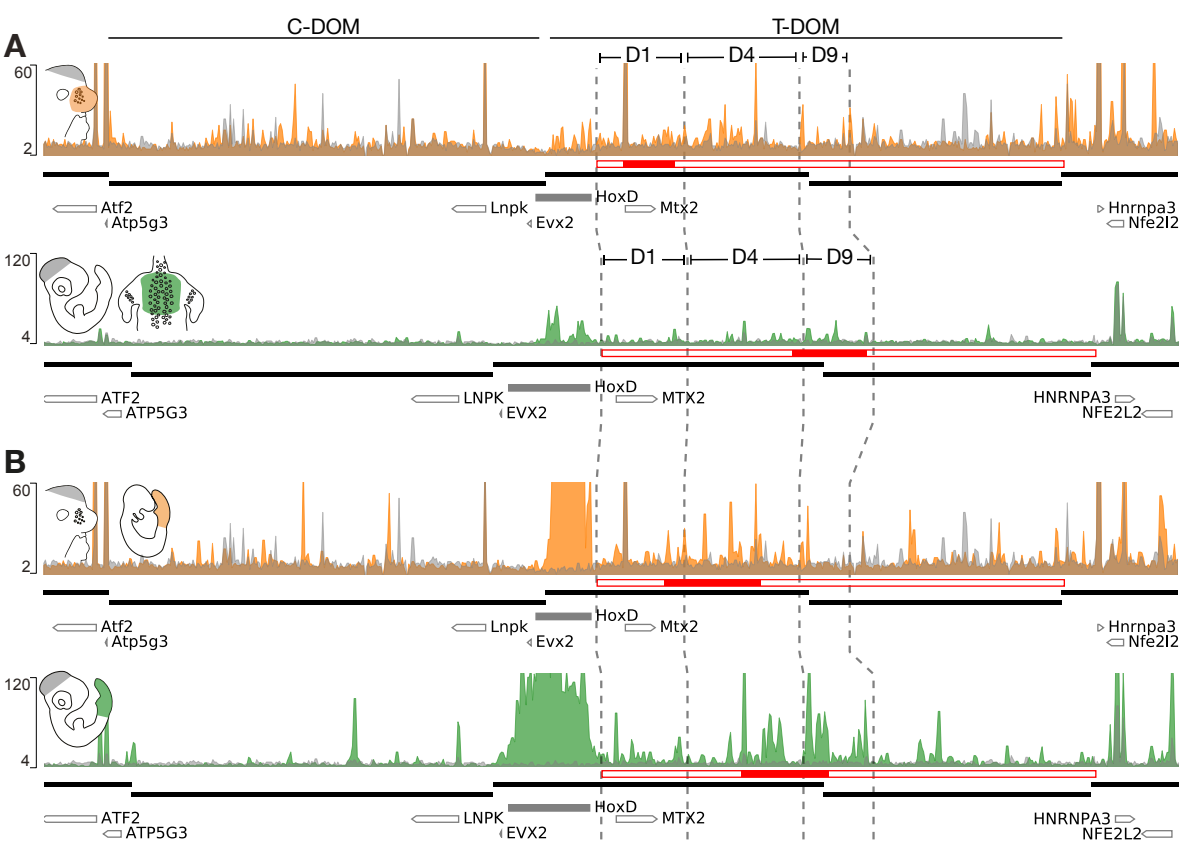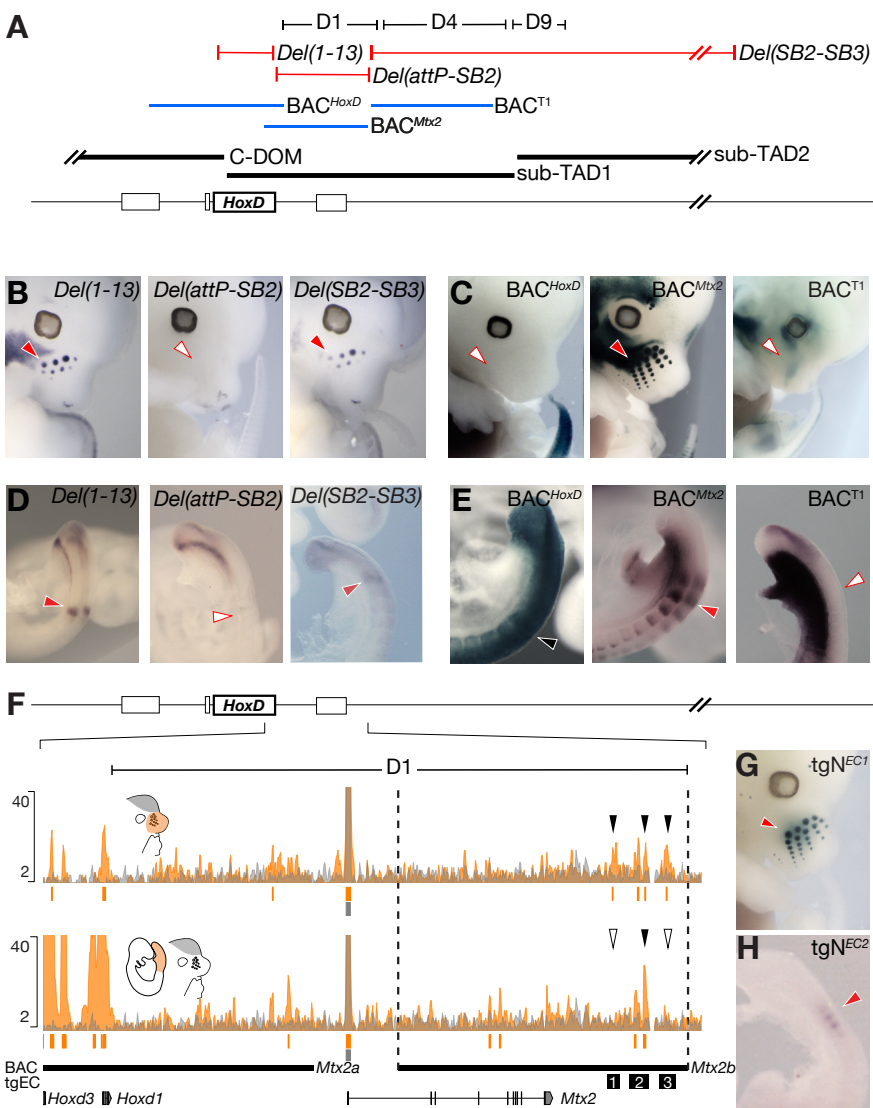1109

Hintermann et al.
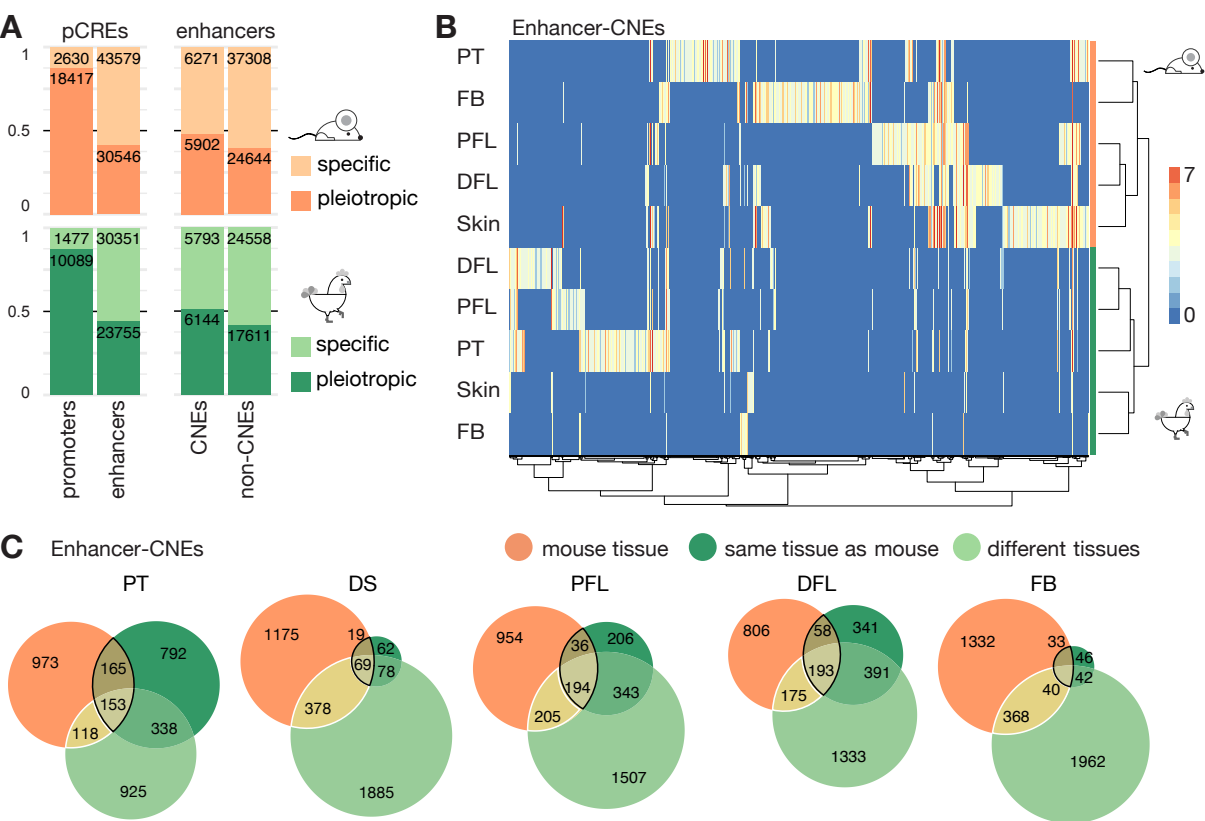Figure 1
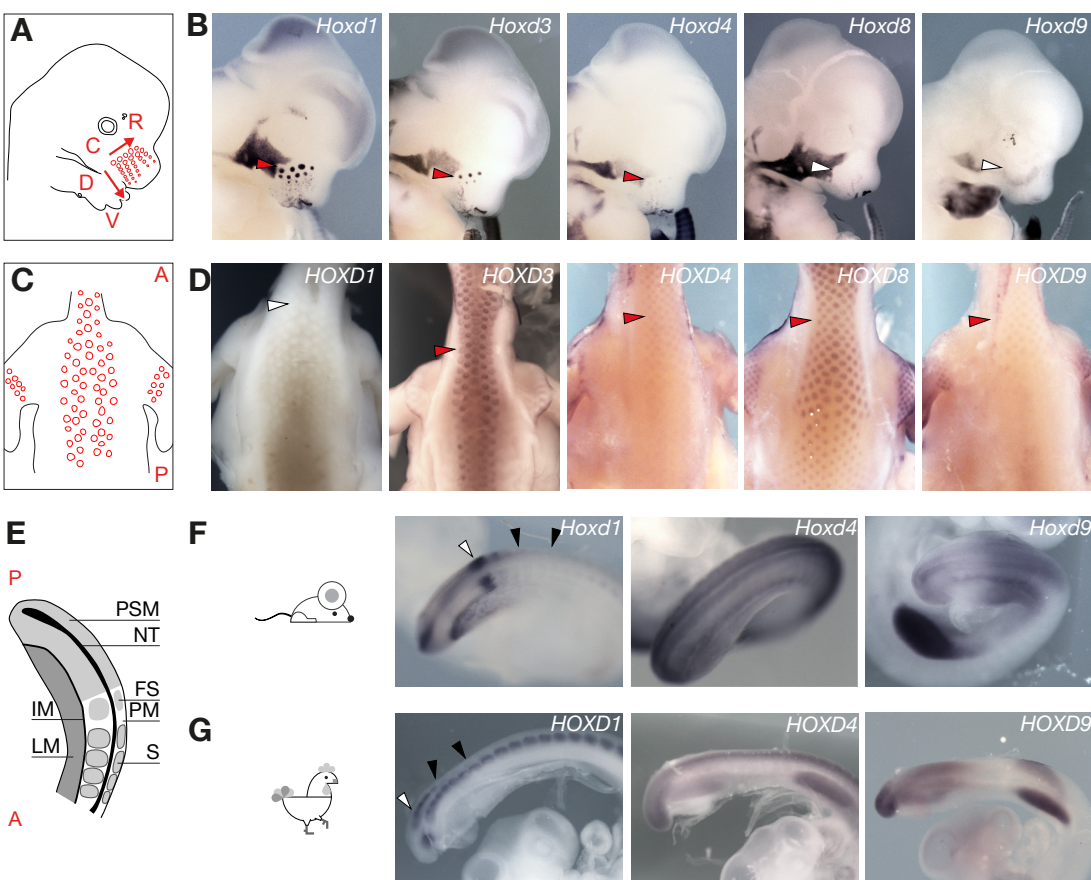
Hintermann et al.
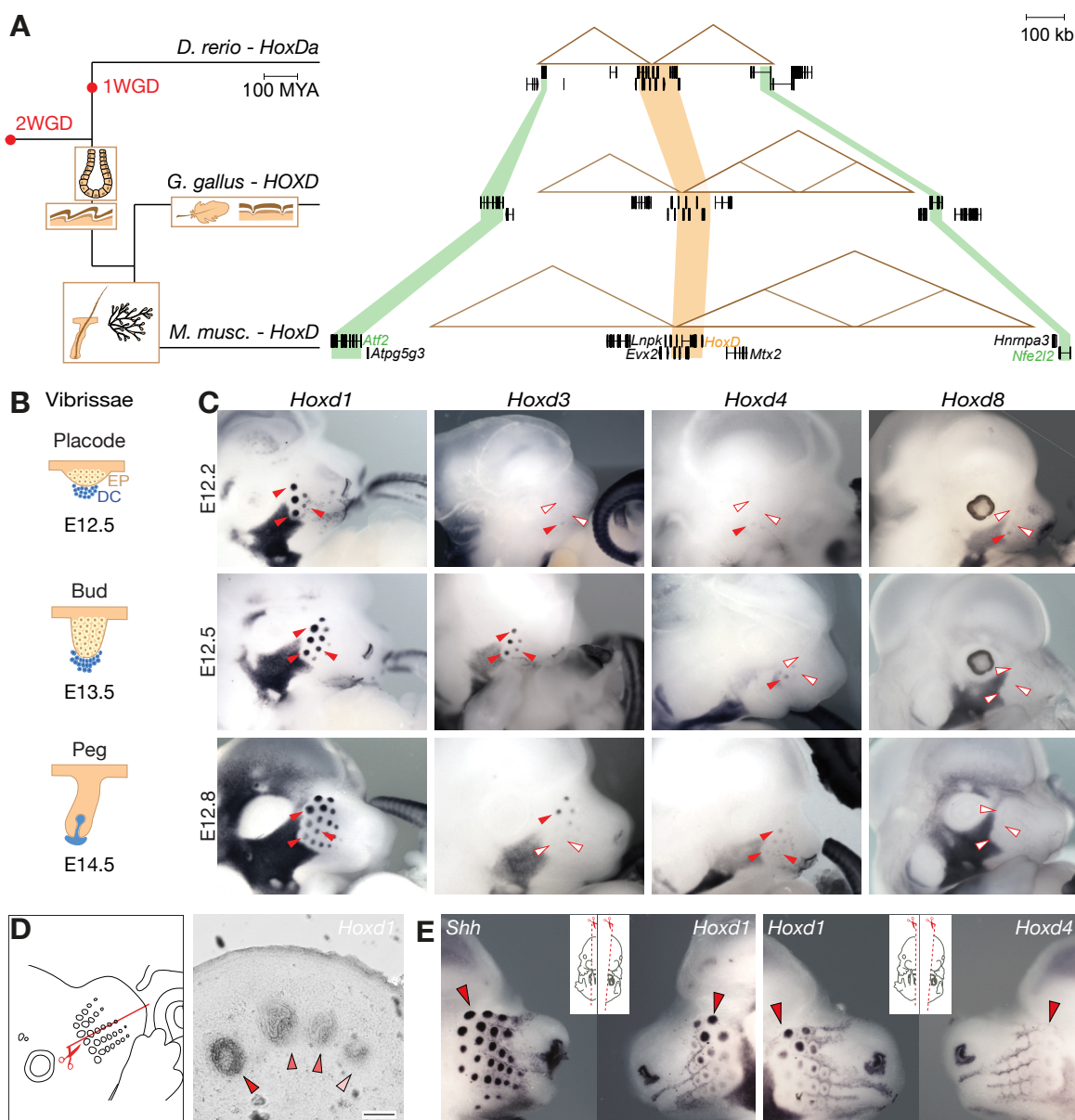Figure 2
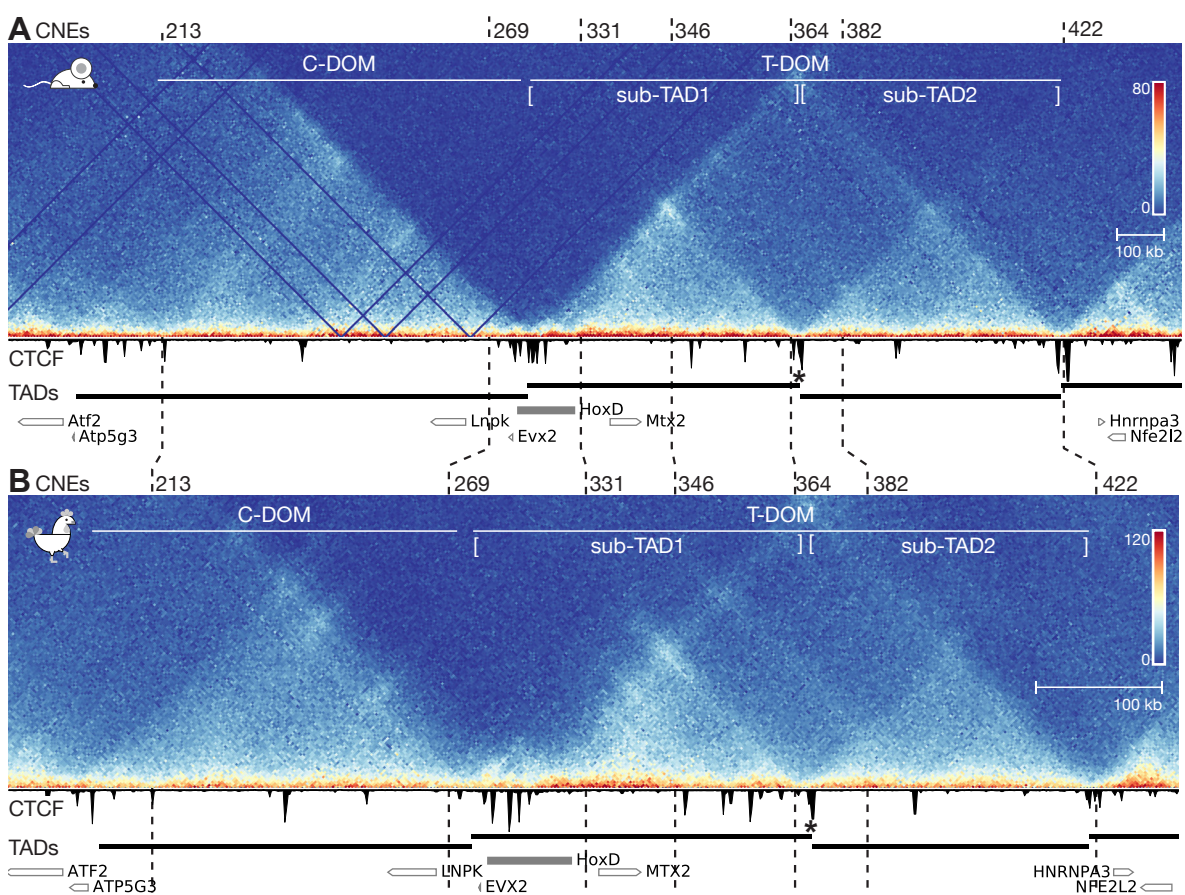
Hintermann et al.
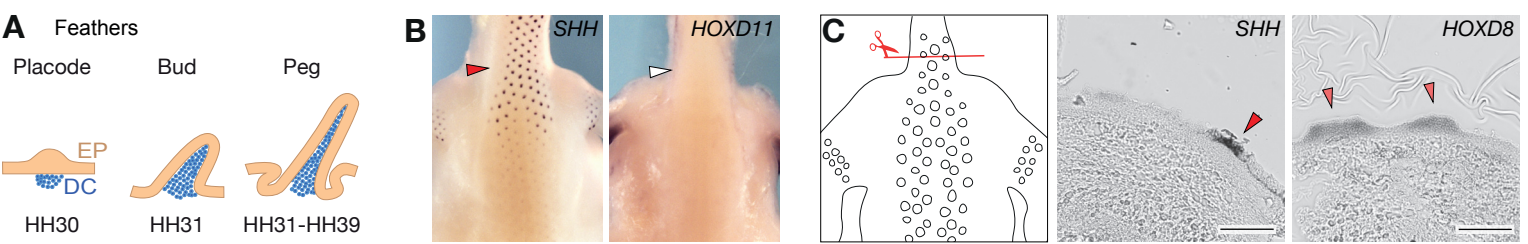Figure 3

Hintermann et al.
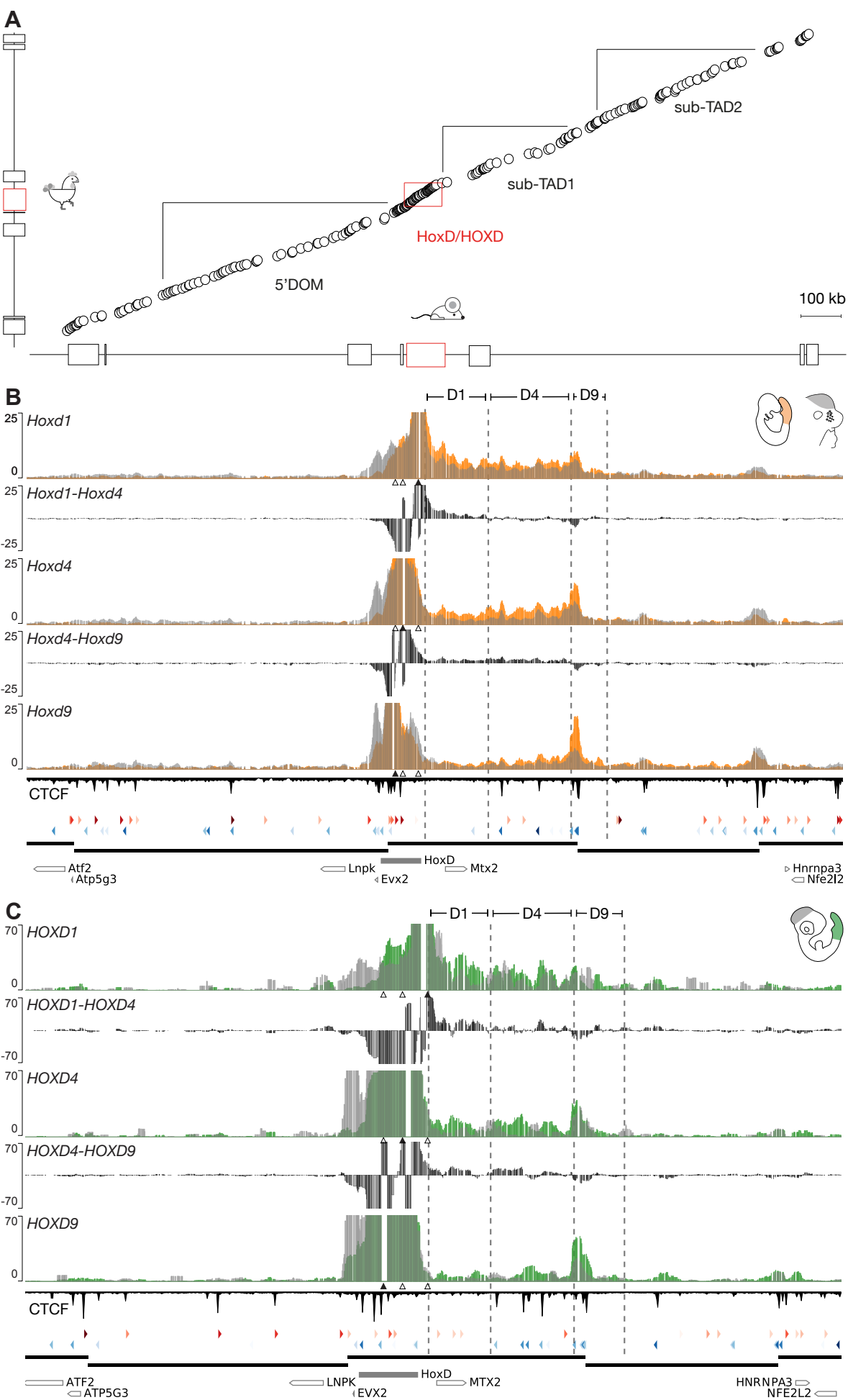Figure 4

Hintermann et al.
Figure 5

Hintermann et al.
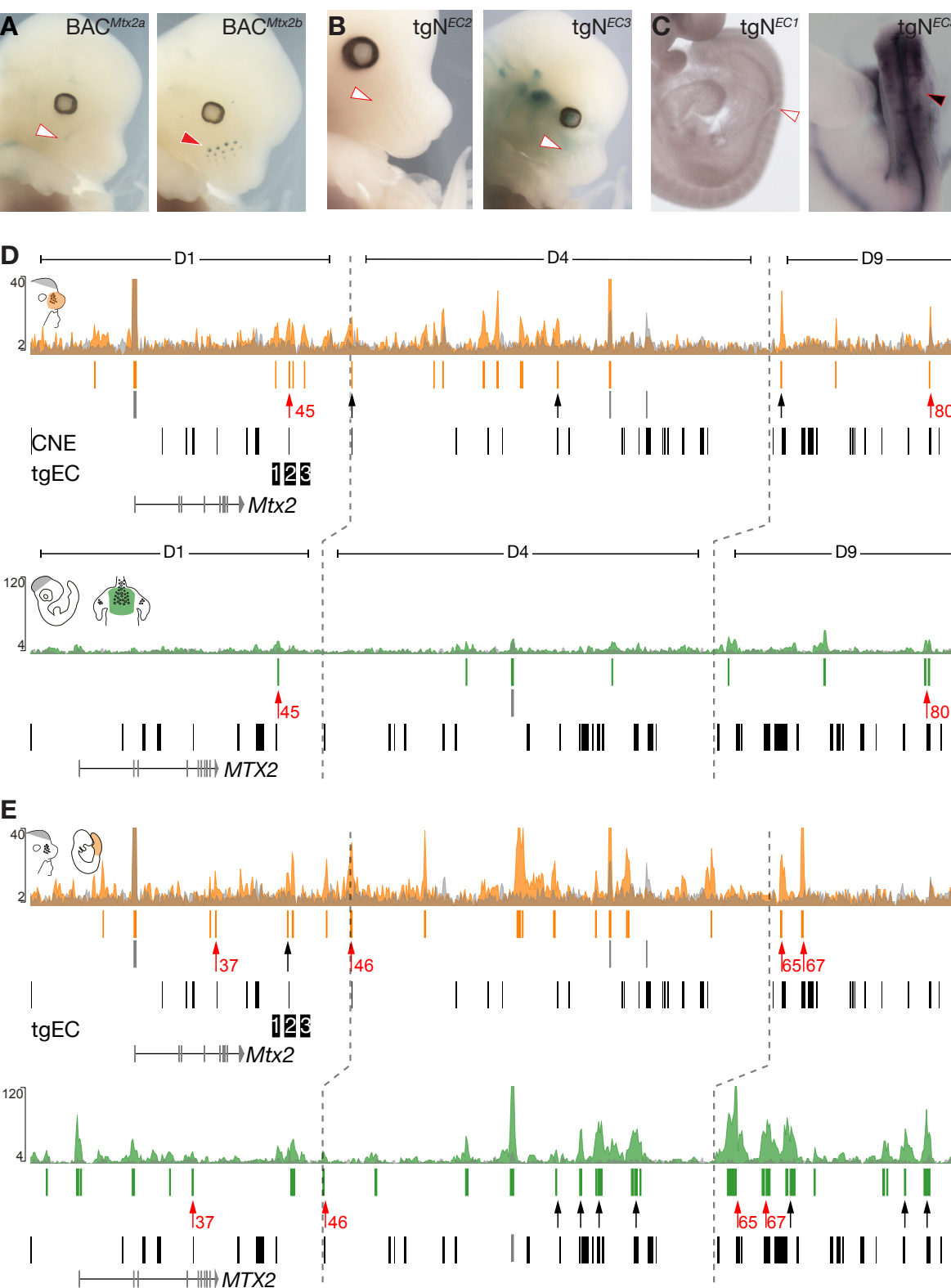Supplementary Figure S1

Hintermann et al.
Supplementary Figure S2

Hintermann et al.
Supplementary Figure S3

Hintermann et al.
Supplementary Figure S4

Supplementary Table 1. List of pre-existing modified mouse lines.

Line	Reference	Coordinates	Primers for genotyping
Del(1-13)d9lac	(Rodriguez-Carballo et al., 2017)	chr2:74663889-74764314	F : GACCGCTTATCCAATTCGGTTC R : CAAGGTCCTCAGCCTTAAGAGTGG
Del(Attp-SB2)	(Andrey et al., 2013)	chr2:74765140-74916570	F: ATCCCGGGGGATCCACTAGAG R: GCTATATAGTAGTTT CAAGGCCAGCCC
Del(Attp-SB3)	(Andrey et al., 2013)	Chr2:74765140-75767350	F: ATCCCGGGGGATCCACTAGAG R: GCTTCCCTAGTTTATGGGGGAGG
Del(SB2-SB3)	(Schep et al., 2016)	chr2:74916560-75767350	F: ATCCCGGGGGATCCACTAGAG R: GCTTCCCTAGTTTATGGGGGAGG
TgBAC^{Mtx2}	(Allais-Bonnet et al., 2021)	chr2:74747769-74913171	
TgBAC^{T1}	BAC1 in (Delpretti et al., 2013)	chr2:74918538-75112340	F: CCTGCTGATGAAGCAGAACA R: CAGCGACCAGATGATCACAC
TgBAC^{T2}	BAC7 in (Delpretti et al., 2013)	chr2:75171805-75354437	
TgBAC^{HoxD}	(Schep et al., 2016)	chr2:74563168-74777972	F: GGTAAACTGGCTCGGATTAGGG R: CTATTCAAAGGTGGGGAGCAGTC

Supplementary Table 2. Primers used to clone enhancer candidates.

CRE name	Coordinates	Primers for cloning
EC1	chr2:74892377-74895558	F : TCCTCTCAAATTTTCCTAACCCCCA R : CCCACCTGCCTCTACATAGCTC
EC2	chr2:74898212-74903231	F : CTGTCACCACCCCAGTCCTG R : AAAAAGGGGGAGTGGGTGGG
EC3	chr2:74905913-74910158	F : AGGTTCCTGTCTTCGTGTTGG R : GTAGCTCACCAGGGCTGAGG

Supplementary Table 3. Probes for *In situ hybridization.*

Mouse

Probe name	Reference	Digestion/ Transcription
Hoxd1	Our laboratory	NcoI / Sp6
Hoxd3	Our laboratory	PmlII / T3
Hoxd4	Our laboratory	EcoRI / Sp6
Hoxd8	Our laboratory	EcoRI / T7
Hoxd9	Our laboratory	BamHI / T7
Shh	Our laboratory	HindIII / T7

Chicken

Probe name / vector (size bp)	Reference	Digestion/ Transcription
HOXD1	Our laboratory	SalI / T7
HOXD3	Our laboratory	SalI / T7
HOXD4	Our laboratory	NcoI / Sp6
HOXD8	Our laboratory	NotI / T3
HOXD9	(Burke et al., 1995)	ClaI / T3
HOXD11	(Burke et al., 1995)	EcoRI / Sp6
SHH	Our laboratory	NcoI / Sp6

References

Allais-Bonnet, A., Hintermann, A., Deloche, M.-C., Cornette, R., Bardou, P., Naval-Sanchez, M., Pinton, A., Haruda, A., Grohs, C., Zakany, J., et al. (2021). Analysis of Polycerate Mutants Reveals the Evolutionary Co-option of *HOXD1* for Horn Patterning in Bovidae. *Molecular Biology and Evolution* 38, 2260–2272.

Andrey, G., Montavon, T., Mascrez, B., Gonzalez, F., Noordermeer, D., Leleu, M., Trono, D., Spitz, F. and Duboule, D. (2013). A switch between topological domains underlies HoxD genes collinearity in mouse limbs. *Science (New York, N.Y.)* 340, 1234167.

Burke, A. C., Nelson, C. E., Morgan, B. A. and Tabin, C. (1995). Hox genes and the evolution of vertebrate axial morphology. *Development* 121, 333–346.

Delpretti, S., Montavon, T., Leleu, M., Joye, E., Tzika, A., Milinkovitch, M. and Duboule, D. (2013). Multiple enhancers regulate Hoxd genes and the Hotdog LncRNA during cecum budding. *Cell reports* 5, 137–50.

Rodriguez-Carballo, E., Lopez-Delisle, L., Zhan, Y., Fabre, P. J., Beccari, L., El-Idrissi, I., Huynh, T. H. N., Ozadam, H., Dekker, J. and Duboule, D. (2017). The HoxD cluster

is a dynamic and resilient TAD boundary controlling the segregation of antagonistic regulatory landscapes. *Genes Dev* 31, 2264–2281.

Schep, R., Necsulea, A., Rodríguez-Carballo, E., Guerreiro, I., Andrey, G., Nguyen Huynh, T. H., Marcet, V., Zákány, J., Duboule, D. and Beccari, L. (2016). Control of Hoxd gene transcription in the mammary bud by hijacking a preexisting regulatory landscape. *Proc. Natl. Acad. Sci. U.S.A.* 113, E7720–E7729.